17th Electromagnetic and Light Scattering Conference
College Station, TX, USA 4–9 March 2018

Numerically Efficient Direct Solver-Based Full-Wave Model for EM Scattering from Complex-Geometry Particles

Ines Fenni*, Ziad S. Haddad*, Hélène Roussel**, Raj Mittra#

* Jet Propulsion Laboratory, California Institute of Technology, USA ** Sorbonne University, L2E-UR, France, # University of Central Florida, USA


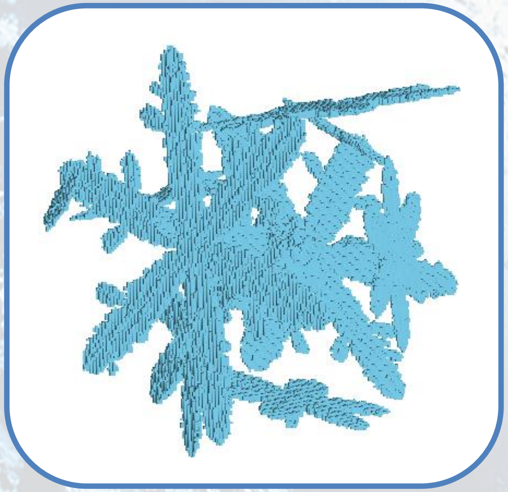


Outline

1) Motivations

- Increasing need for **accurate and numerically efficient** model of EM scattering from **particles of arbitrary geometry and composition.**
- Limitations of **iterative solvers-based** Discrete Dipole Approximation (**DDA**) codes

2) VIEM-MoM/CBFM

- **VIEM/MoM**-based 3D full wave model for **scattering by complex-shaped precipitation particles**.
- Application of the domain decomposition-based **CBFM**

3) Numerical Analysis

- Primary Validation of **NESCoP** by comparison to **Mie theory**
- Application of **NESCoP vs DDSCat** to different types of **complex-geometry and electrically large particles**

EM Scattering by arbitrarily shaped particles

Z. S. Haddad & al, "Derived Observations From Frequently Sampled Microwave Measurements of Precipitation—Part I: Relations to Atmospheric Thermodynamics," in IEEE Transactions on Geoscience and Remote Sensing, June 2017.

NEED Single-scattering properties of particles with complex arbitrary geometries modeling **ice pristine and snowflakes**.

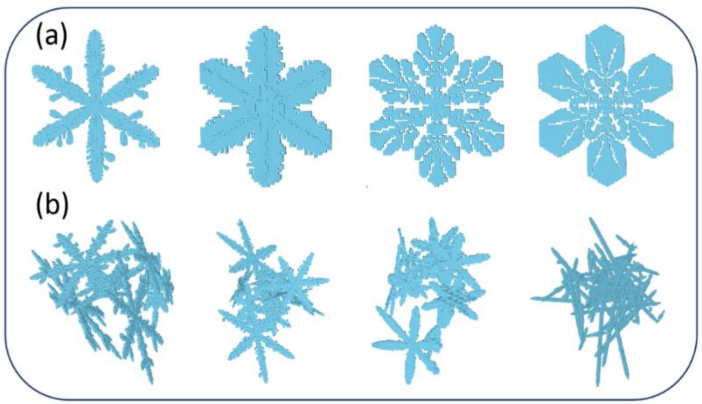

Pristine crystals (a) & aggregate (b) snow particles from OpenSSP database

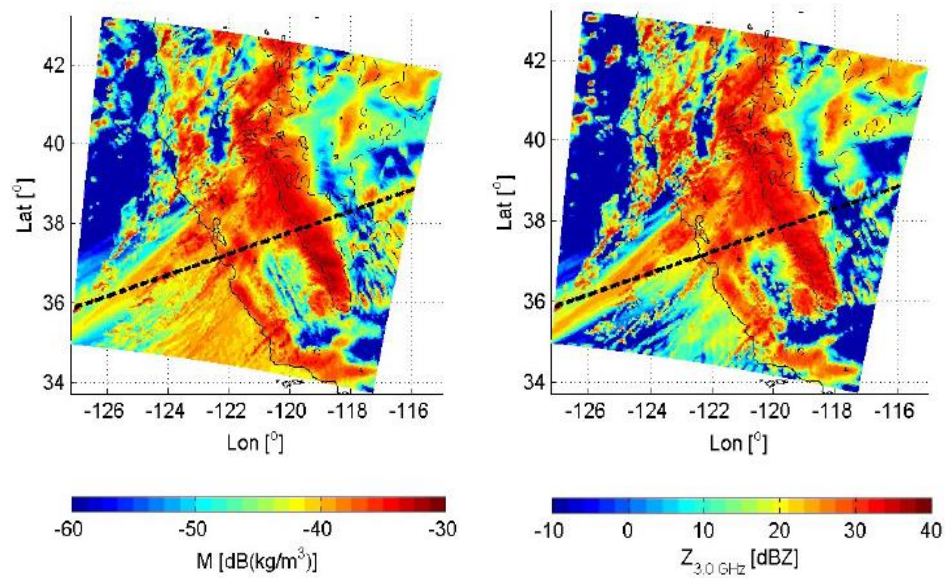

WRF simulations of the California blizzard : maps of condensed-water mass and S-band radar reflectivity

Scattering Lookup Tables ➡

$$Z(x,h) = \sum_{i=1}^{N_{\text{species}}} \boxed{Z_{u,i}(x,h)} \times \exp\left[-2 \int_h^{\infty} \sum_{j=1}^{N_{\text{species}}} \boxed{k_{\text{ext},j}(x,h')} dh' \right]$$

EM Scattering by arbitrarily shaped particles

Mollon, Guilhem, and Jidong Zhao. "3D generation of realistic granular samples based on random fields theory and Fourier shape descriptors." Computer Methods in Applied Mechanics and Engineering 2014.

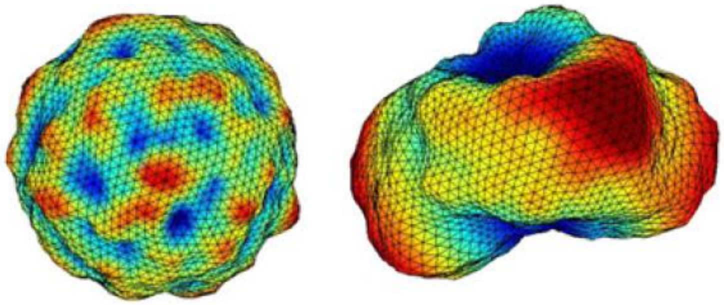

Mishchenko, Michael I., and Janna M. Dlugach. "Radar polarimetry of Saturn's rings: Modeling ring particles as fractal aggregates built of small ice monomers." Journal of Quantitative Spectroscopy and Radiative Transfer 2009

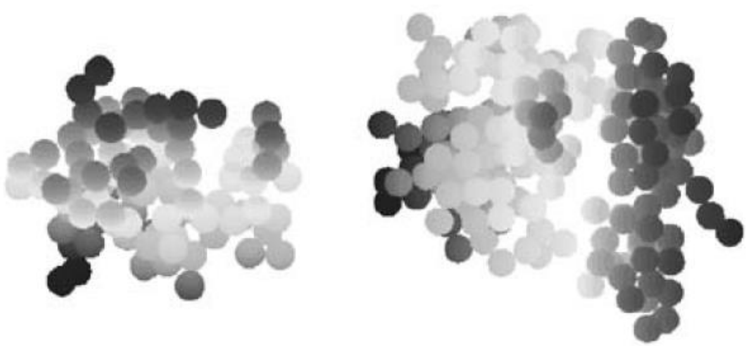

NEED

Single-scattering properties of particles with complex arbitrary geometries.

Different types of particles in nature : **mineral aerosol** particles in planetary atmospheres, **cosmic dust** particles, **regolith** particles on the surface of terrestrial planets and asteroids, **ice-cloud** particles…

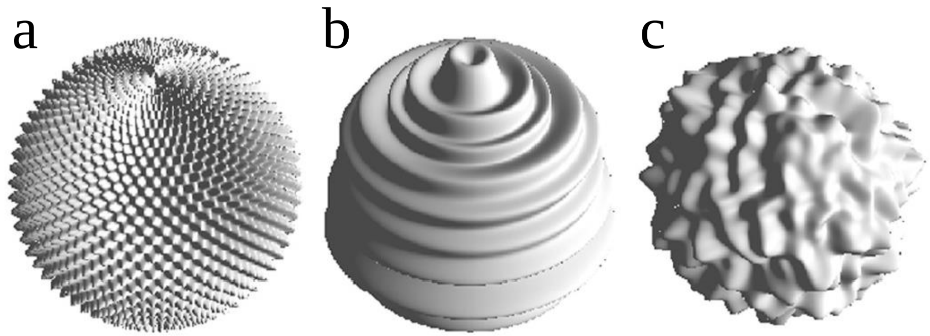

(a) 3D Chebyshev particles, (b) 2D and (c) 3D Gaussian random spheres

Kahnert, Michael, et al. "Light scattering by particles with small-scale surface roughness: comparison of four classes of model geometries." Journal of Quantitative Spectroscopy and Radiative Transfer, 2012.

EM Scattering by arbitrarily shaped particles

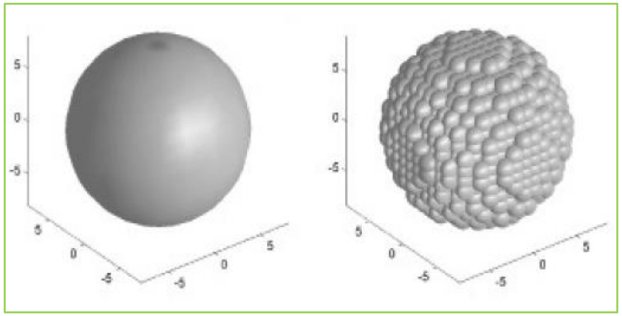

Discrete dipole approximation (DDA) representation of a sphere

Single-scattering properties of particles with complex arbitrary geometries.

Discrete Dipole approximation (DDA) : DDScat, ADDA, SIRRI, …

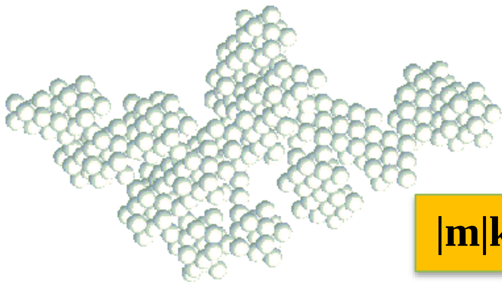

$|m|kd = 0.6$

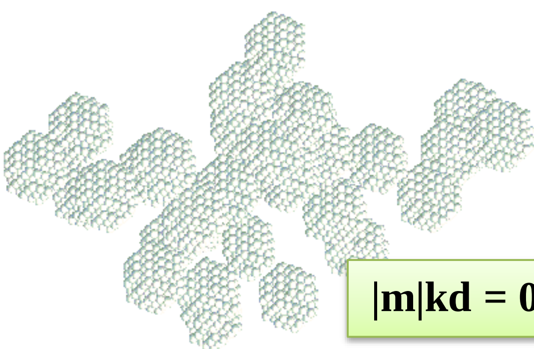

$|m|kd = 0.26$

Validity criteria : $|m|kd \leq 1$

- **m** : complex refractive index
- **k** : wavelength number
- **d** : grid spacing

B.T. Draine and P.J. Flatau, "Discrete-dipole approximation for scattering calculations," in JOSA A, 1994.

Penttilä, Antti, et al. "Comparison between discrete dipole implementations and exact techniques." *JQSRT,* 2007

Zubko, Evgenij, et al. "Validity criteria of the discrete dipole approximation." Applied optics, 2010

EM Scattering by arbitrarily shaped particles

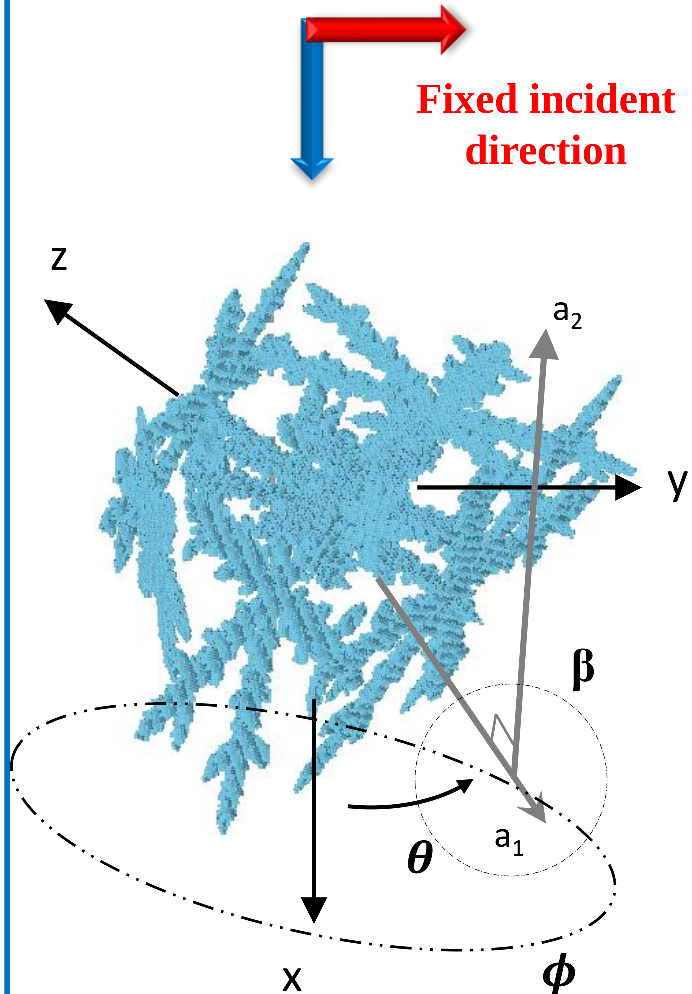

Single-scattering properties of particles with complex arbitrary geometries.

Discrete Dipole approximation (DDA) : DDScat, ADDA, SIRRI, …

Iterative solvers : Krylov-space methods, such as conjugate gradient (**CG**), Bi-CG, Bi-CG stabilized (**Bi-CGSTAB**), CG squared (**CGS**), generalized minimal residual (GMRES),

Orientation averaging

$$\langle \boldsymbol{Q} \rangle = \frac{\mathbf{1}}{\mathbf{8}\boldsymbol{\pi}^{\mathbf{2}}} \int_{0}^{2\pi} d\boldsymbol{\beta} \int_{-1}^{1} \boldsymbol{d} \cos \boldsymbol{\theta} \int_{0}^{2\pi} \boldsymbol{d\phi}\ \boldsymbol{Q}(\boldsymbol{\beta}, \boldsymbol{\theta}, \boldsymbol{\phi})$$

Yurkin, Maxim A., and Alfons G. Hoekstra. "The discrete dipole approximation: an overview and recent developments." Journal of Quantitative Spectroscopy and Radiative Transfer, 2007

EM Scattering by arbitrarily shaped particles

Fixed orientation of the particle

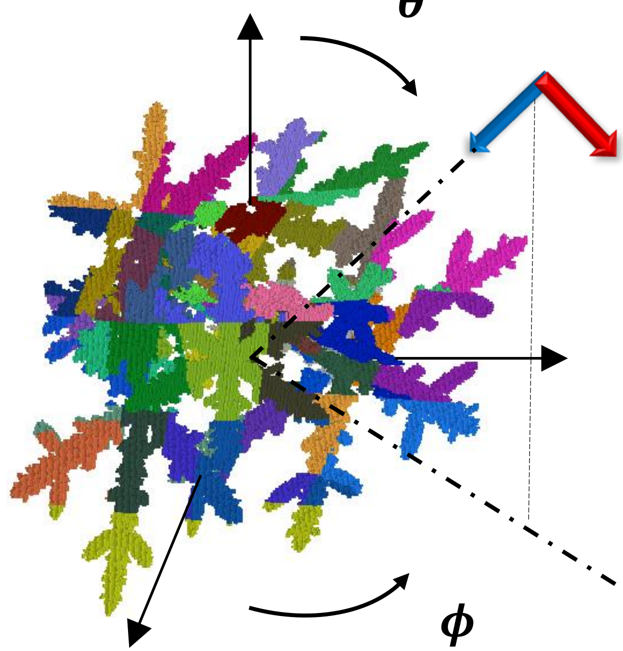

$$\boldsymbol{Z E = E^{inc}}$$

Direct solver

Single-scattering properties of electrically large and complex-geometry particles.

Discrete Dipole approximation
(**DDA**) : DDScat, ADDA, SIRRI, …

Characteristic Basis Function Method
(Domain decomposition method)

Orientation averaging

$$\langle Q \rangle = \frac{1}{4\pi} \int_0^{2\pi} d\phi_i \int_0^{\pi} \sin\theta_i \; d\theta_i \, Q(\phi_i, \theta_i)$$

Singham, M. K., Shermila B. Singham, and Gary C. Salzman. "The scattering matrix for randomly oriented particles." *The Journal of chemical physics* 85.7 (1986)

The Characteristic Basis Function Method (CBFM)

Direct solver-based

- **B**etter adapted to **multiple right-hand** side problem
- **S**ubject to a wide variety of enhancement techniques
- **T**unable depending on to the needs (memory or CPU) through the size of the blocks (h_B or $N_{b,max}$).
- **H**ighly amenable to **MPI** parallelization

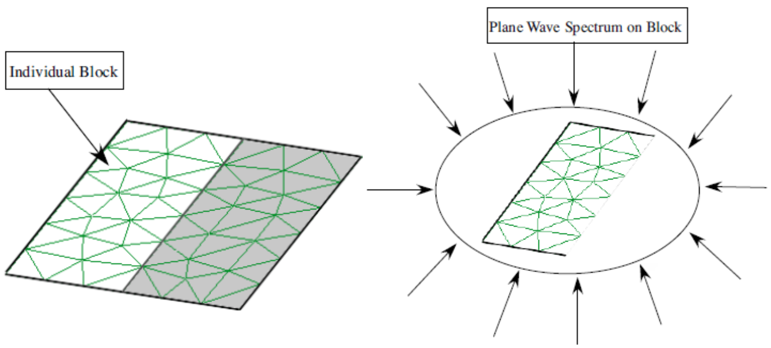

Spectrum of plane waves incident on a single block

R. Maaskant, R. Mittra, A. Tijhuis, "Fast Analysis of Large Antenna Arrays Using the Characteristic Basis Function Method and the Adaptive Cross Approximation Algorithm", IEEE Transactions on Antennas and Propagation, 2008.

Jaime Laviada et al,"Solution of Electrically Large Problems With Multilevel Characteristic Basis Functions", IEEE Trans. on Antennas Propagation, 2009.

The **CBFM** which has been proven to be accurate and efficient when applied to large-scale EM problems, even when the computational resources are limited

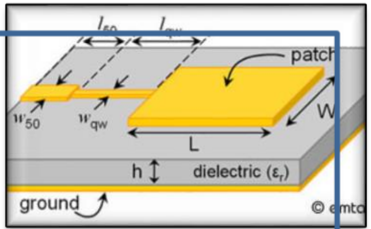

Microstrip circuits

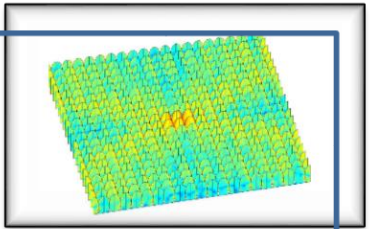

Large antenna arrays

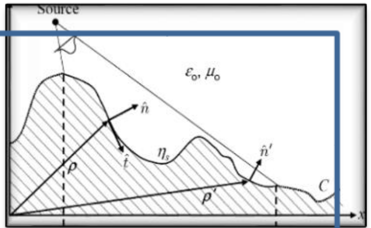

Rough terrain profiles

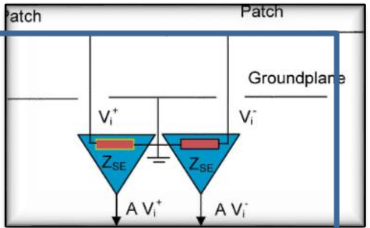

Connected patch arrays

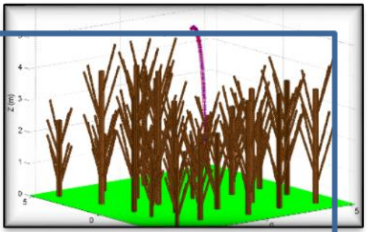

Bodies of revolution (BoRs)

Outline

2) VIEM-MoM/CBFM

- **VIEM/MoM**-based 3D full wave model for **scattering by complex-shaped precipitation particles**.
- Application of the domain decomposition-based **CBFM**

3) Numerical Analysis

- Primary Validation of **NESCoP** by comparison to **Mie theory**
- Application of **NESCoP vs DDSCat** to different types of **complex-geometry and electrically large particles**

VIEM/MoM-based 3D full-wave model

3D full-wave model, based on the volume integral equation method (VIEM)

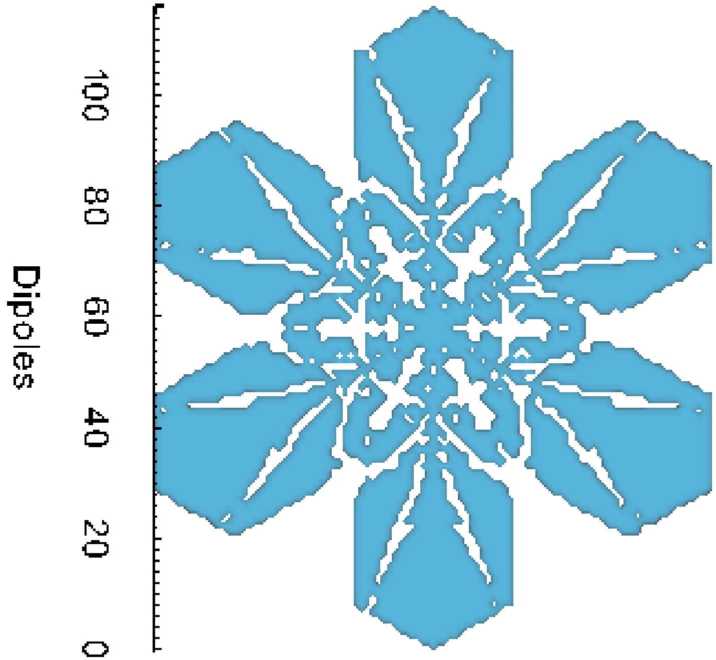

Pristine crystal particle

where $\chi(\bar{r}')$ is the dielectric contrast at the location r', k_0 is the wavenumber in air and $\bar{\bar{G}}(\bar{r},\bar{r}')$ is the free space dyadic Green's function.

VIEM : $$\bar{E}(\bar{r}) = \bar{E}^{inc}(\bar{r}) + \left(k_0^2 + \nabla\nabla.\right)\int_{\Omega} \chi(\bar{r}')\, \bar{\bar{G}}(\bar{r},\bar{r}')\, \bar{E}(\bar{r}')\, d\bar{r}'$$

$$\boxed{\bar{\bar{\Gamma}}\bar{E}(\bar{r}) = \bar{E}^{ref}(\bar{r})}$$ where $$\bar{\bar{\Gamma}} = \bar{\bar{I}} - \left(k_0^2 + \nabla\nabla.\right)\int_{\Omega} \chi(\bar{r}')\, \bar{\bar{G}}(\bar{r},\bar{r}')\, d\bar{r}'$$

VIEM/MoM-based 3D full-wave model

3D full-wave model, based on the volume integral equation method (VIEM)

Pristine crystal particle
discretized into Nb_c
elementary cubic cells

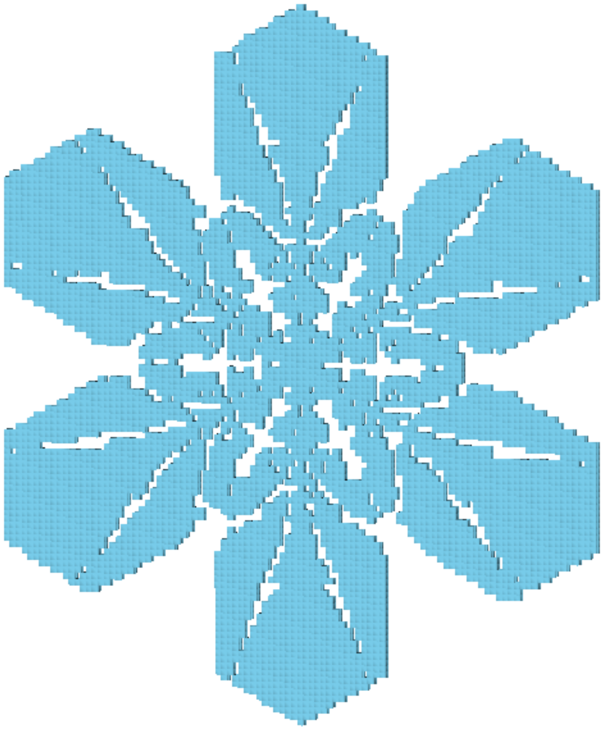

$$\bar{\bar{\Gamma}}\bar{E}(\bar{r}) = \bar{E}^{ref}(\bar{r})$$

Method of Moments

The particle is discretized into **Nbc** cubic cells Ω_n ,of side S_c

$$S_c \le \frac{\lambda_s}{10}\ ;\ \lambda_s = \frac{\lambda_0}{\sqrt{Re(\varepsilon_r)}}$$

$$D_\lambda = \lambda_s / S_c$$

Z is the **$3Nb_c$** x **$3Nb_c$ full** matrix representing the **interactions** between the different cells.

$$\bar{E}(\bar{r}) = \sum_{n=1}^{N}\sum_{q=1}^{3} E_q^n\ \bar{F}_q^n(\bar{r})$$

Use of piecewise constant basis functions

$$Z\ E = E^{inc}$$

VIEM/MoM-based 3D full-wave model

3D full-wave model, based on the volume integral equation method (VIEM)

Pristine crystal particle discretized into Nb_c elementary cubic cells

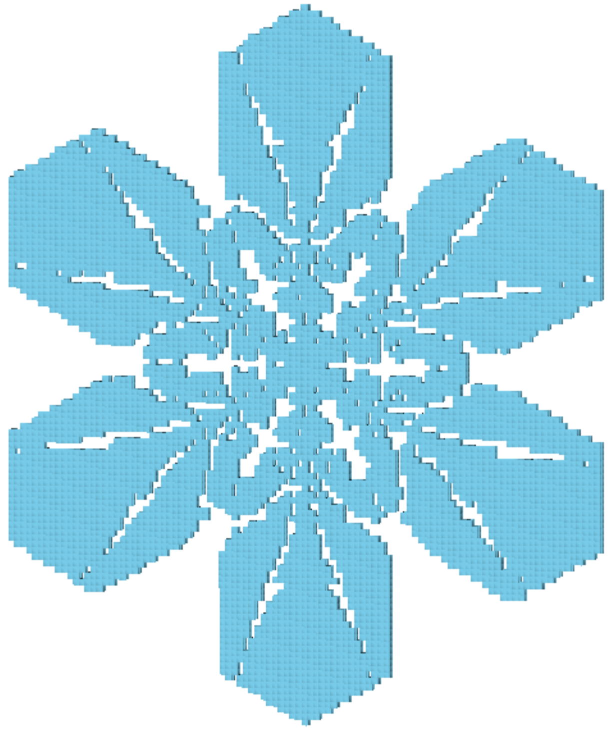

Z is the **$3Nb_c$** x **$3Nb_c$ full** matrix representing the **interactions** between the different cells.

$$\bar{\bar{\Gamma}}\bar{E}(\bar{r}) = \bar{E}^{ref}(\bar{r})$$

Method of Moments

The particle is discretized into **Nbc** cubic cells Ω_n ,of side S_c

$$S_c \leq \frac{\lambda_s}{10} \; ; \lambda_s = \frac{\lambda_0}{\sqrt{Re(\varepsilon_r)}}$$

$$D_\lambda = \lambda_s / S_c$$

$$\bar{E}(\bar{r}) = \sum_{n=1}^{N}\sum_{q=1}^{3} E_q^n \, \bar{F}_q^n(\bar{r})$$

Use of piecewise constant basis functions

$$Z\,E = E^{inc}$$

3D full-wave model, based on the volume integral equation method (VIEM)

Pristine crystal particle discretized into Nb_c elementary cubic cells

Z is the **$3Nb_c$** x **$3Nb_c$ full** matrix representing the **interactions** between the different cells.

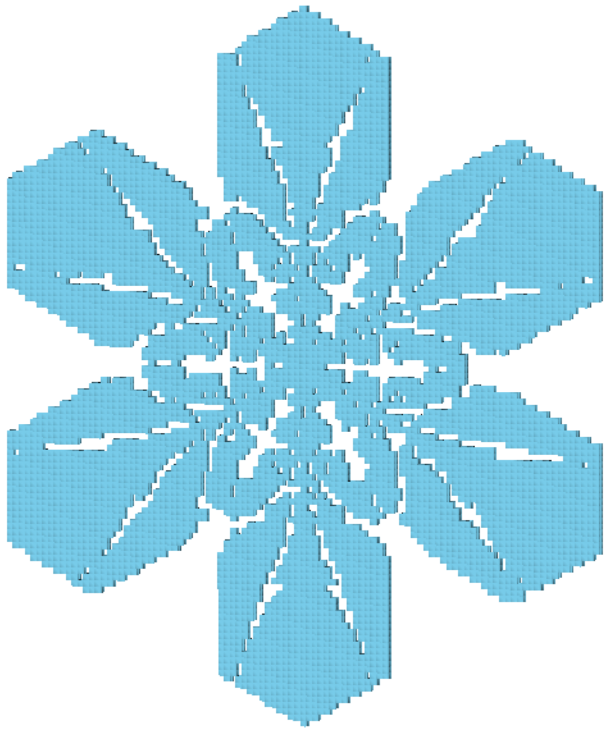

$$\bar{\bar{\Gamma}}\bar{E}(\bar{r}) = \bar{E}^{ref}(\bar{r})$$

Method of Moments

The particle is discretized into **Nbc** cubic cells Ω_n ,of side S_c

$$S_c \leq \frac{\lambda_s}{10} \; ; \lambda_s = \frac{\lambda_0}{\sqrt{Re(\varepsilon_r)}}$$

$$D_\lambda = \lambda_s / S_c$$

$$\bar{E}(\bar{r}) = \sum_{n=1}^{N}\sum_{q=1}^{3} E_q^n \, \bar{F}_q^n(\bar{r})$$

Use of piecewise constant basis functions

CBFM

$$Z\,E = E^{inc}$$

Application of the domain decomposition-based CBFM

After dividing the 3D complex geometry of the precipitation particle of N cells into M blocks

1 Generation of the CBFs

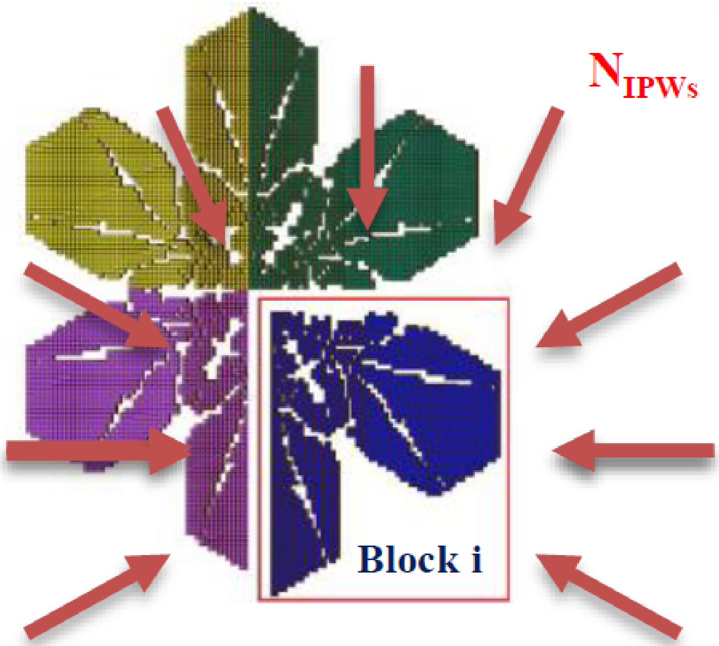

$$\color{red}{Z^{ii}}\, E^{i}_{MBFs} = E^{i}_{IPWs}$$

$$E^i = \begin{pmatrix} E_1^{(i,\theta_1,\varphi_1)} & E_1^{(i,\theta_2,\varphi_1)} & \cdots & E_1^{(i,\theta_{N\theta},\varphi_1)} & E_1^{(i,\theta_1,\varphi_2)} & \cdots & E_1^{(i,\theta_{N\theta},\varphi_{N\varphi})} \\ E_2^{(i,\theta_1,\varphi_1)} & E_2^{(i,\theta_2,\varphi_1)} & \cdots & E_2^{(i,\theta_{N\theta},\varphi_1)} & E_2^{(i,\theta_1,\varphi_2)} & \cdots & E_2^{(i,\theta_{N\theta},\varphi_{N\varphi})} \\ E_3^{(i,\theta_1,\varphi_1)} & E_3^{(i,\theta_2,\varphi_1)} & \cdots & E_3^{(i,\theta_{N\theta},\varphi_1)} & E_3^{(i,\theta_1,\varphi_2)} & \cdots & E_3^{(i,\theta_{N\theta},\varphi_{N\varphi})} \\ \vdots & \vdots & \ddots & \vdots & \vdots & \ddots & \vdots \\ E_{N_i}^{(i,\theta_1,\varphi_1)} & E_{N_i}^{(i,\theta_2,\varphi_1)} & \cdots & E_{N_i}^{(i,\theta_{N\theta},\varphi_1)} & E_{N_i}^{(i,\theta_1,\varphi_2)} & \cdots & E_{N_i}^{(i,\theta_{N\theta},\varphi_{N\varphi})} \end{pmatrix}$$

$3N_i$ (rows) × N_{IPWs} (columns)

Singular Value Decomposition (SVD)

+

Normalization and thresholding (10^{-3})

=

S_i characteristic basis functions (CBFs) for the block i

Application of the domain decomposition-based CBFM

After dividing the 3D complex geometry of the precipitation particle of N cells into M blocks

1 **Generation of the CBFs**

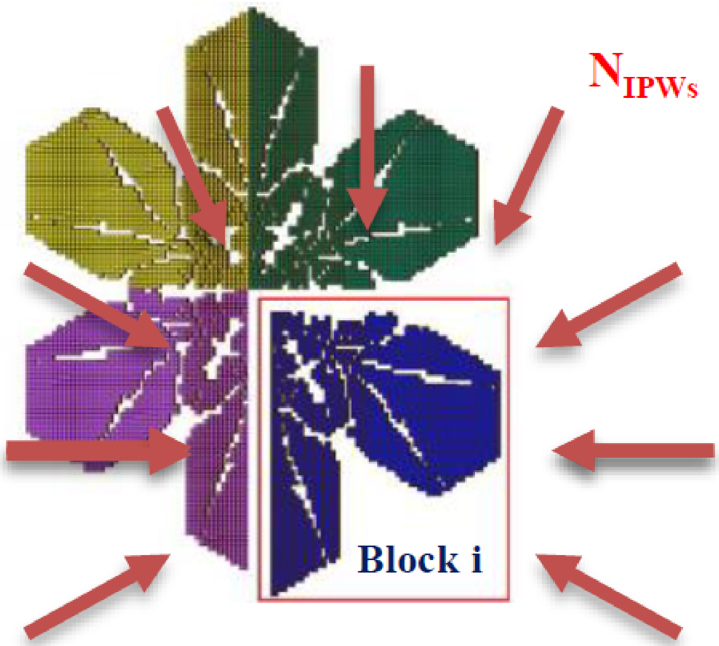

$$Z^{ii} E^{i}_{MBFs} = E^{i}_{IPWs}$$

2 **Computation of Z^c**

Example : M = 4

$$Z^c = \begin{pmatrix} C^{(1)t} Z_{11} C^{(1)} & \cdots & C^{(1)t} Z_{14} C^{(4)} \\ C^{(2)t} Z_{21} C^{(1)} & \cdots & C^{(2)t} Z_{24} C^{(4)} \\ \vdots & \ddots & \vdots \\ C^{(4)t} Z_{41} C^{(1)} & \cdots & C^{(4)t} Z_{44} C^{(4)} \end{pmatrix}$$

$$K = S_1 + S_2 + S_3 + S_4 \ll 3{*}N$$

3

$$\boxed{Z^c \alpha = E^{c,inc}}$$

Application of the domain decomposition-based CBFM

After dividing the 3D complex geometry of the precipitation particle of N cells into M blocks

1 Generation of the CBFs

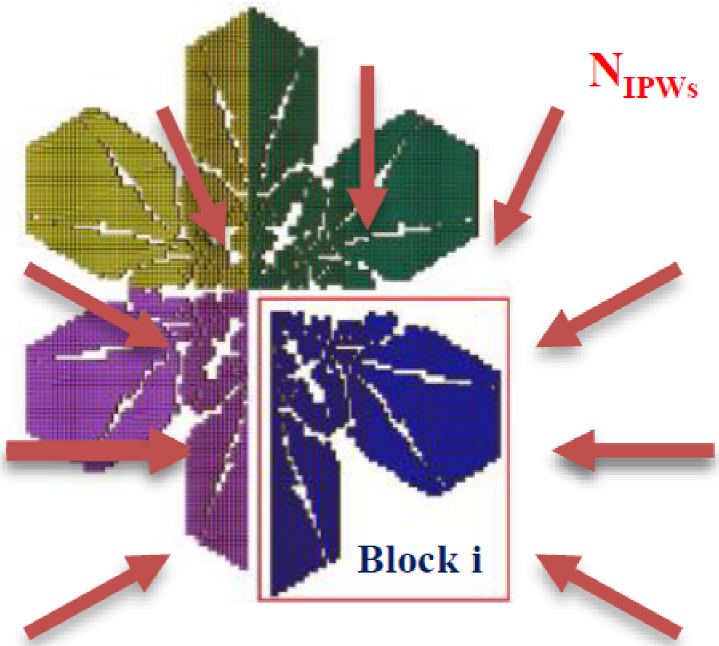

$$Z^{ii} E^{i}_{MBFs} = E^{i}_{IPWs}$$

2 Computation of Z^c

Example : M = 4

$$Z^c = \begin{pmatrix} C^{(1)t} Z_{11} C^{(1)} & \cdots & C^{(1)t} Z_{14} C^{(4)} \\ C^{(2)t} Z_{21} C^{(1)} & \cdots & C^{(2)t} Z_{24} C^{(4)} \\ \vdots & \ddots & \vdots \\ C^{(4)t} Z_{41} C^{(1)} & \cdots & C^{(4)t} Z_{44} C^{(4)} \end{pmatrix}$$

$$K = S_1 + S_2 + S_3 + S_4 \ll 3*N$$

Compression Rate

$$CR = \frac{\textit{size of } Z}{\textit{size of } Z^c}$$

Application of the domain decomposition-based CBFM

MoM/CBFM in terms of computing complexity

MoM : $O(3N)^3$

CBFM

CBFs : $O(3N/M)^3$

Z^c : $O(3N \times K)$

$(Z^c)^{-1}$: $O(K)^3$

Multilevel

Sparse

MPI

ACA/FMM

Efficient direct

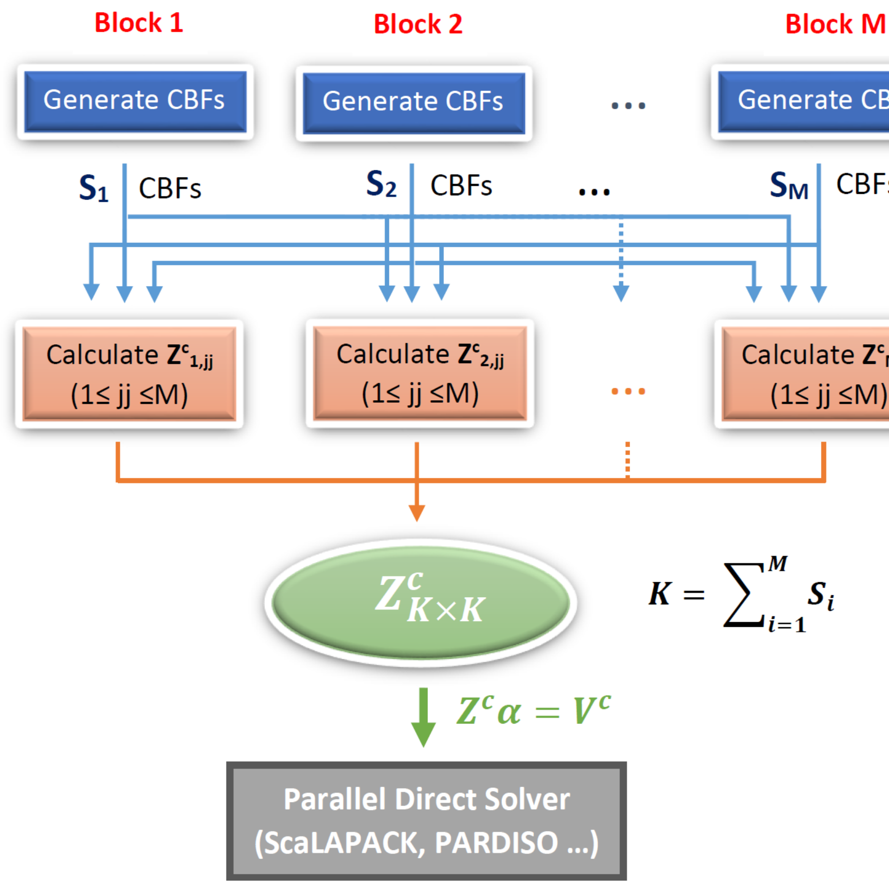

The main steps of the CBFM in a distributed memory parallel configuration

Outline

3) Numerical Analysis

- Primary Validation of **NESCoP** by comparison to **Mie theory**
- Application of **NESCoP vs DDSCat** to different types of **complex-geometry and electrically large particles**

Numerical Analysis : NESCoP vs DDScat

Orientational averaging

N $\langle Q\rangle = \frac{1}{4\pi}\int_0^{2\pi} d\phi_i \int_0^{\pi} \sin\theta_i \, d\theta_i \, Q(\phi_i, \theta_i)$

Incident directions (**id**) – (**θ , ϕ**)

D $\langle Q\rangle = \frac{1}{8\pi^2}\int_0^{2\pi} d\beta \int_{-1}^{1} d\cos\theta \int_0^{2\pi} d\phi \; Q(\beta, \theta, \phi)$

Target orientations (**to**) – (**θ , β**)

Scattering Efficiency Coefficients

$Q_{ext} = C_{ext} / \pi a^2$

$Q_{sca} = C_{sca} / \pi a^2$

$Q_{bks} = C_{bks} / \pi a^2$

$$\begin{pmatrix} E_{\|sca} \\ E_{\perp sca} \end{pmatrix} = \frac{\exp(ik_{sca}r)}{-ik_{sca}r} \begin{pmatrix} S_2 & S_3 \\ S_4 & S_1 \end{pmatrix} \begin{pmatrix} E_{\|in} \\ E_{\perp in} \end{pmatrix}$$

Shared Memory / OpenMP

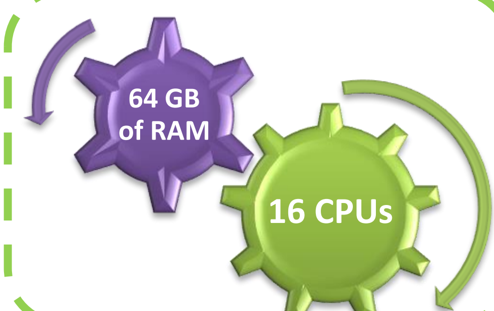

Relative 'difference'

(per frequency)

$$E_{r,t}(\%) = 100 \times \frac{|Q_{t,NESCoP} - Q_{t,DDScat}|}{|Q_{t,DDScat}|}$$

Numerical Analysis : NESCoP vs DDScat vs Mie

Sphere

a_p = 0.8 mm; 17 ≤ f ≤ 200 GHz; m = 1.78 + i 0.00133

703id/900to

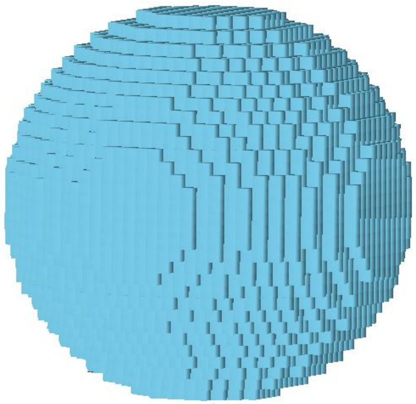

d = 50 µm; |m|kd ≤ 0.38

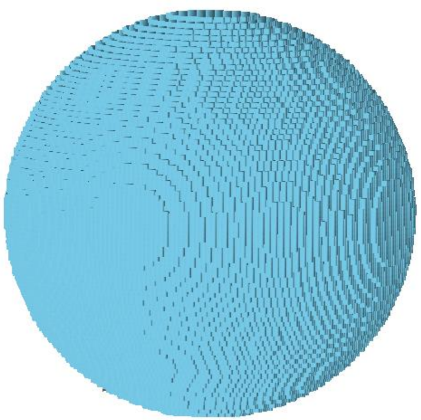

d = 20 µm; |m|kd ≤ 0.15

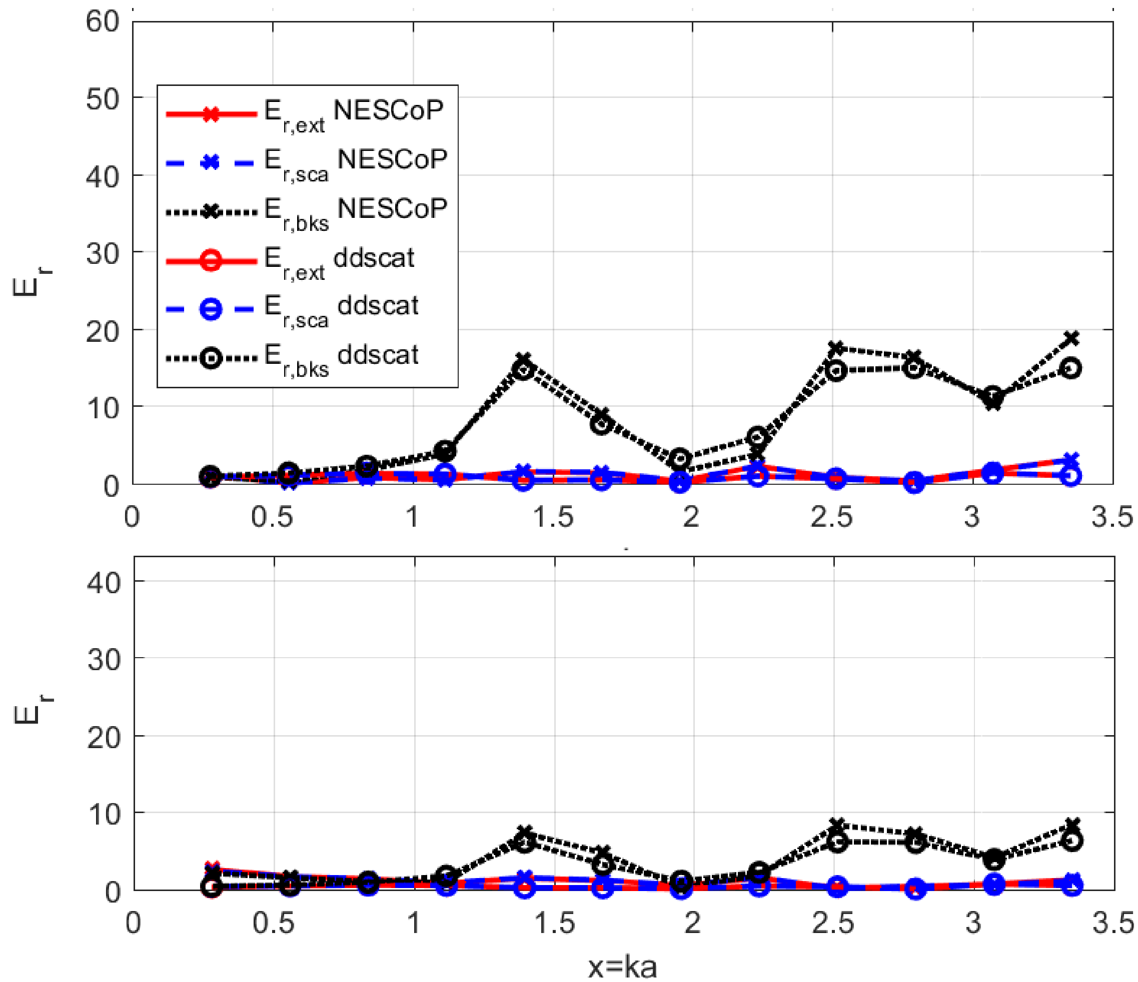

Numerical Analysis : NESCoP vs DDScat vs Mie

Sphere

a_p = 1.9 mm; 17 ≤ f ≤ 200 GHz; m = 1.78 + i 0.00133

1id/1to

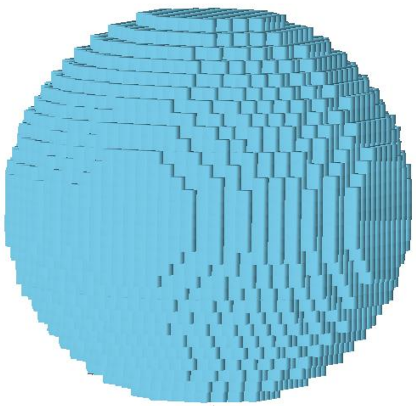

d = 50 µm; |m|kd ≤ 0.38

Iterative solver

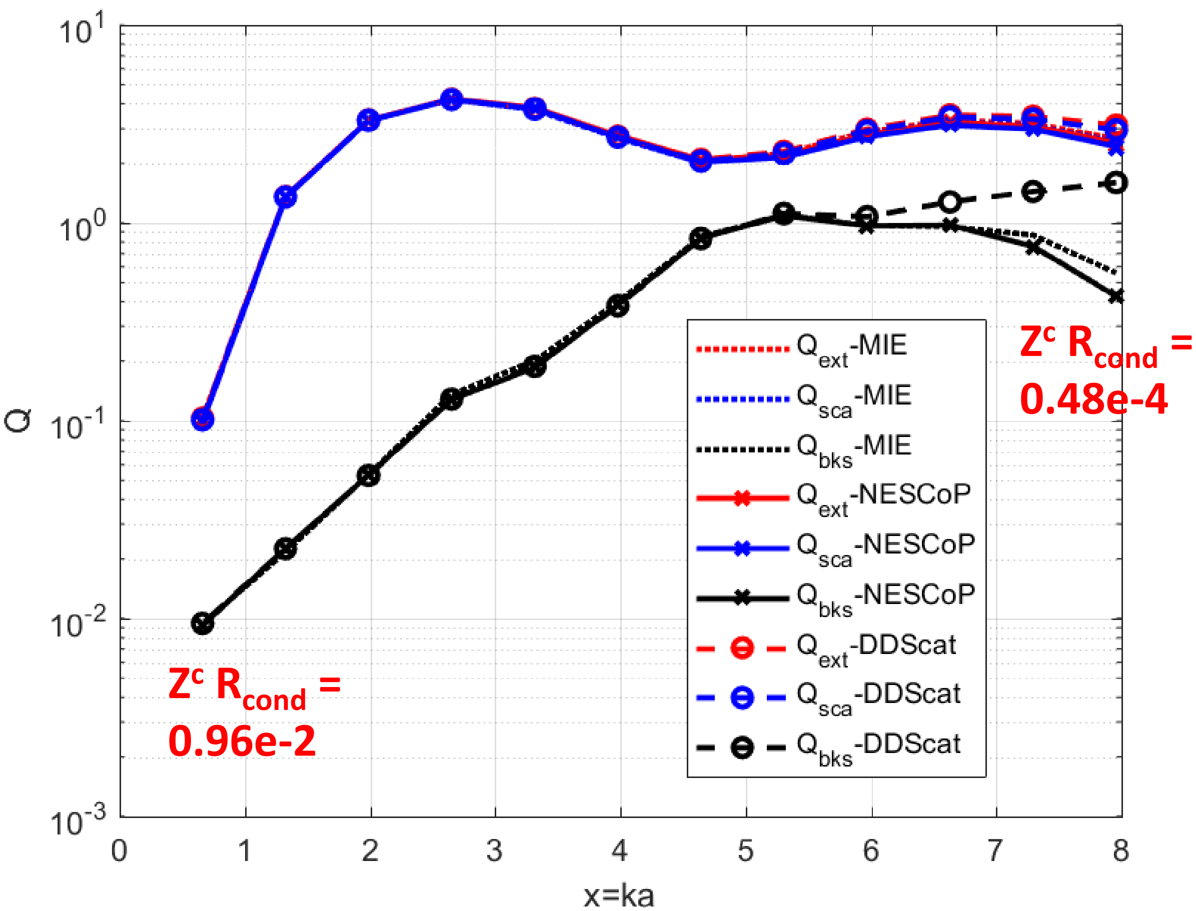

Numerical Analysis : NESCoP vs DDScat vs Mie

Sphere

a_p = 1.9 mm; 17 ≤ f ≤ 200 GHz; m = 1.78 + i 0.00133

1id/1to

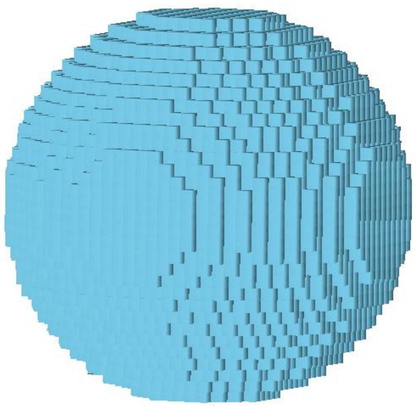

d = 50 µm; |m|kd ≤ 0.38

Iterative solver

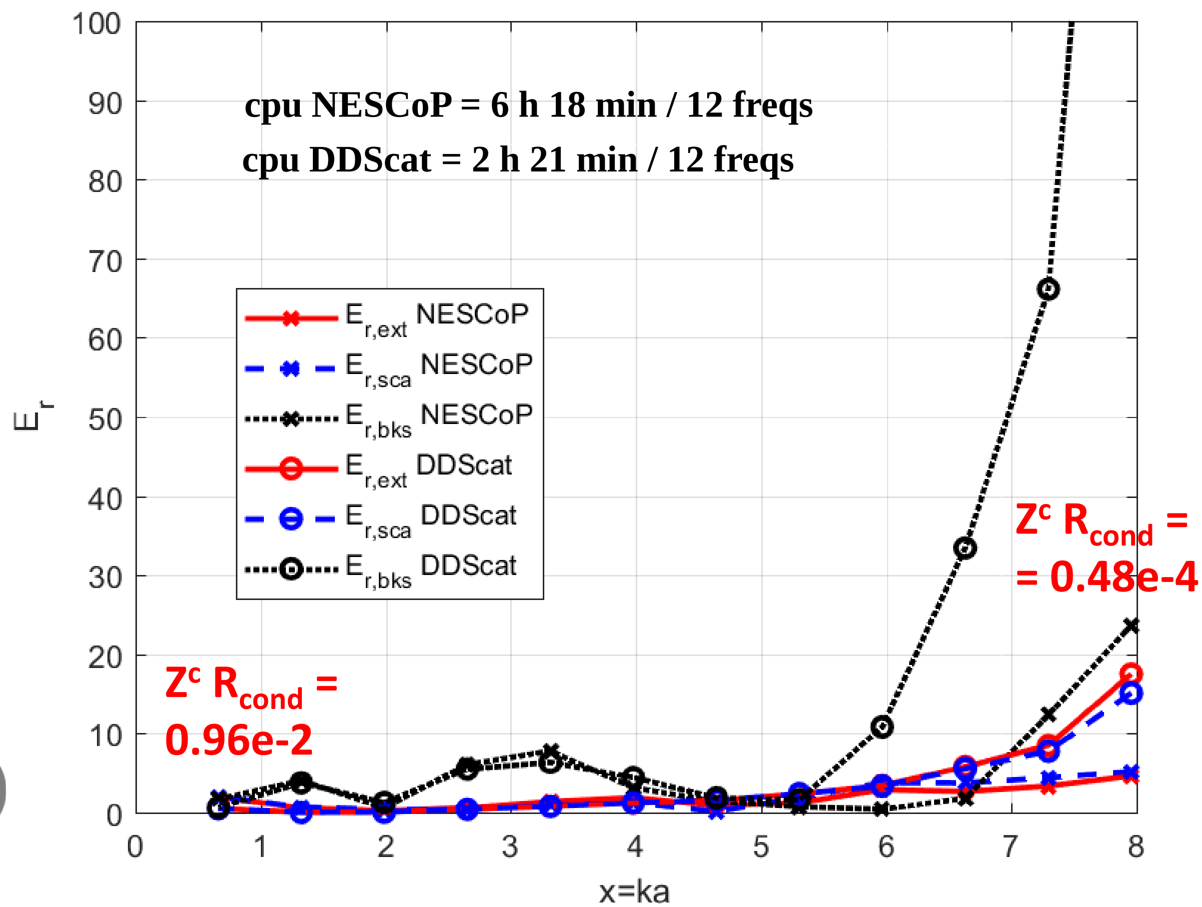

Numerical Analysis : NESCoP vs DDScat vs Mie

Sphere

$a_p = 1.9$ mm; $m = 1.78 + i\ 0.00133$ | $d = 50\ \mu m$; $Nb_c = 229423$ | **1id/1to**

f = 100 GHz; |m|kd = 0.18; x = 3.14

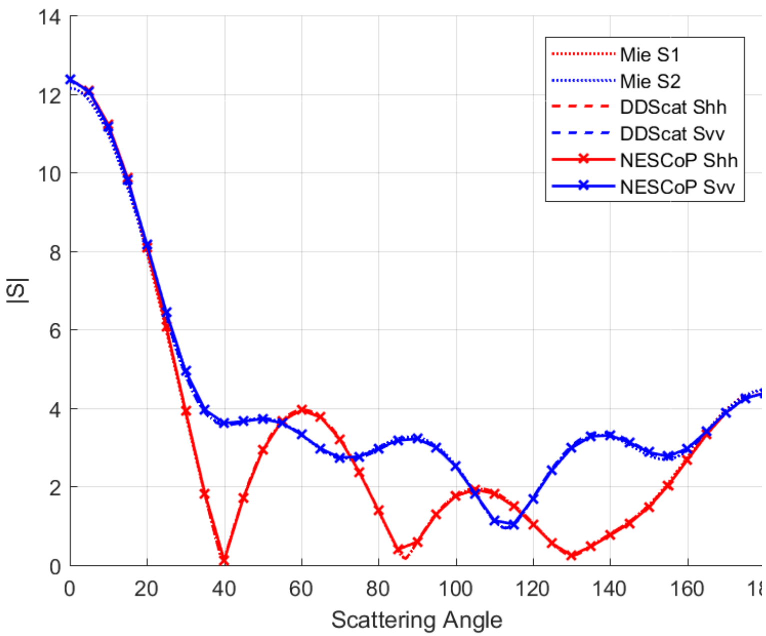


```
>ZBCG2   IT=       31 f.err= 3.726E-05
>ZBCG2   IT=       32 f.err= 4.769E-06
>TIMEIT  Timing results for: PBCGS2
>TIMEIT  1555.523 = CPU time (sec)
```

f = 200 GHz; |m|kd = 0.37; x = 7.96

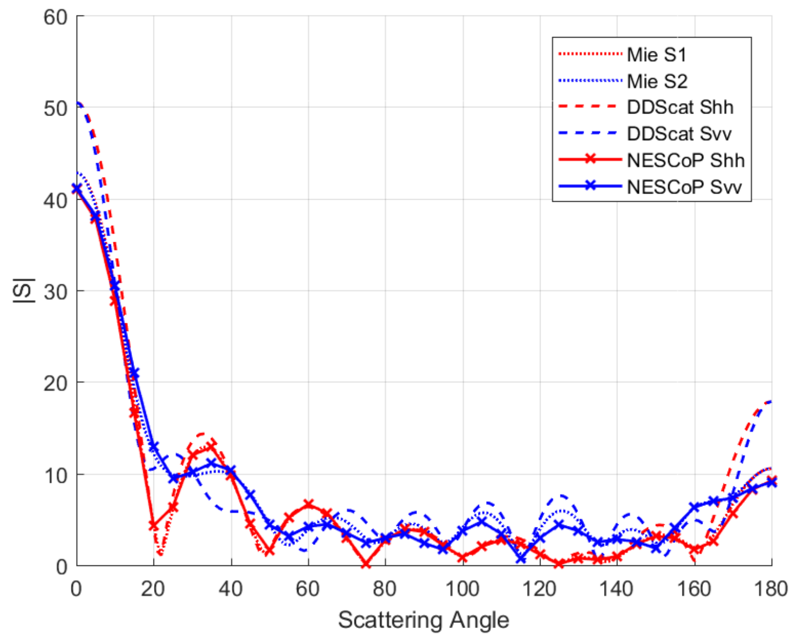


```
>ZBCG2   IT=      538 f.err= 1.119E-05
>ZBCG2   IT=      539 f.err= 9.469E-06
>TIMEIT  Timing results for: PBCGS2
>TIMEIT   25824. = CPU time (sec)
```

Numerical Analysis : NESCoP vs DDScat vs Mie

Sphere

$a_p = 1.9$ mm; $m = 1.78 + i\,0.00133$ $d = 50\ \mu m$; $Nb_c = 229423$ **1id/1to**

f = 100 GHz; |m|kd = 0.18; x = 3.14

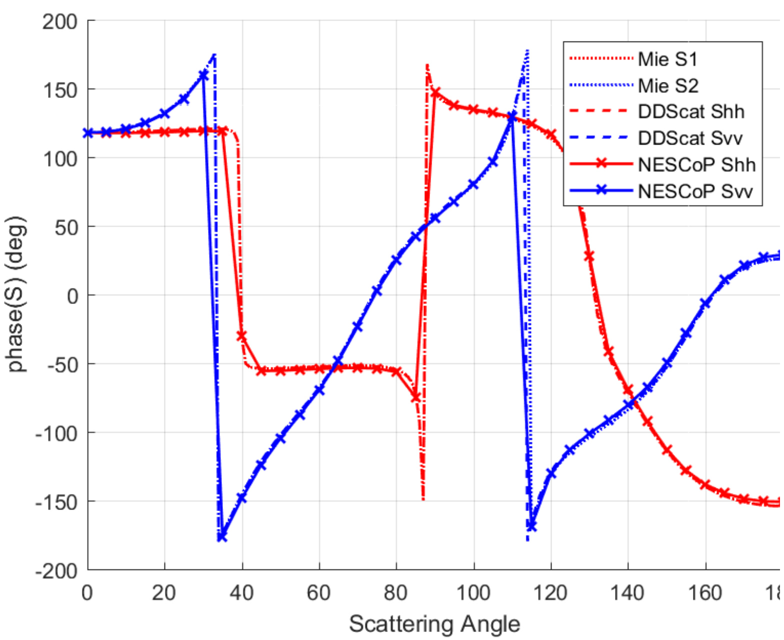


```
>ZBCG2   IT=       31 f.err= 3.726E-05
>ZBCG2   IT=       32 f.err= 4.769E-06
>TIMEIT  Timing results for: PBCGS2
>TIMEIT  1555.523 = CPU time (sec)
```

f = 200 GHz; |m|kd = 0.37; x = 7.96

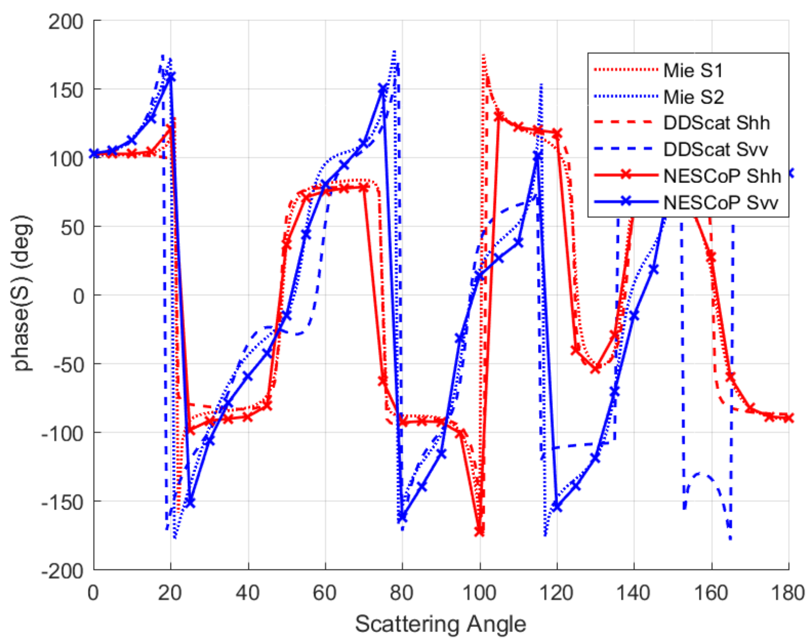


```
>ZBCG2   IT=      538 f.err= 1.119E-05
>ZBCG2   IT=      539 f.err= 9.469E-06
>TIMEIT  Timing results for: PBCGS2
>TIMEIT   25824. = CPU time (sec)
```

Numerical Analysis : NESCoP vs DDScat vs Mie

Sphere

$a_p = 1.9$ mm; $m = 1.78 + i\,0.00133$ $d = 50\ \mu m$; $Nb_c = 229423$ **1id/1to**

f = 100 GHz; |m|kd = 0.18; x = 3.14

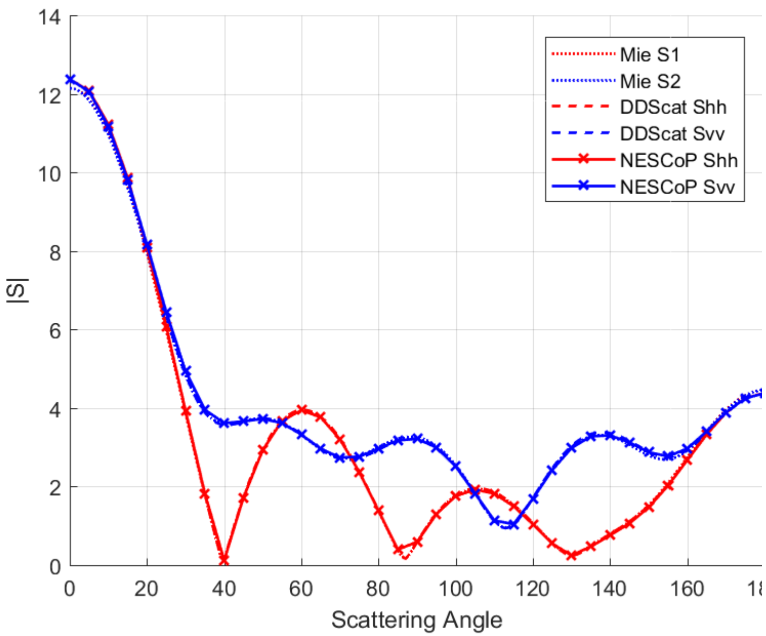


```
>ZBCG2   IT=       31 f.err= 3.726E-05
>ZBCG2   IT=       32 f.err= 4.769E-06
>TIMEIT  Timing results for: PBCGS2
>TIMEIT  1555.523 = CPU time (sec)
```

f = 200 GHz; |m|kd = 0.37; x = 7.96

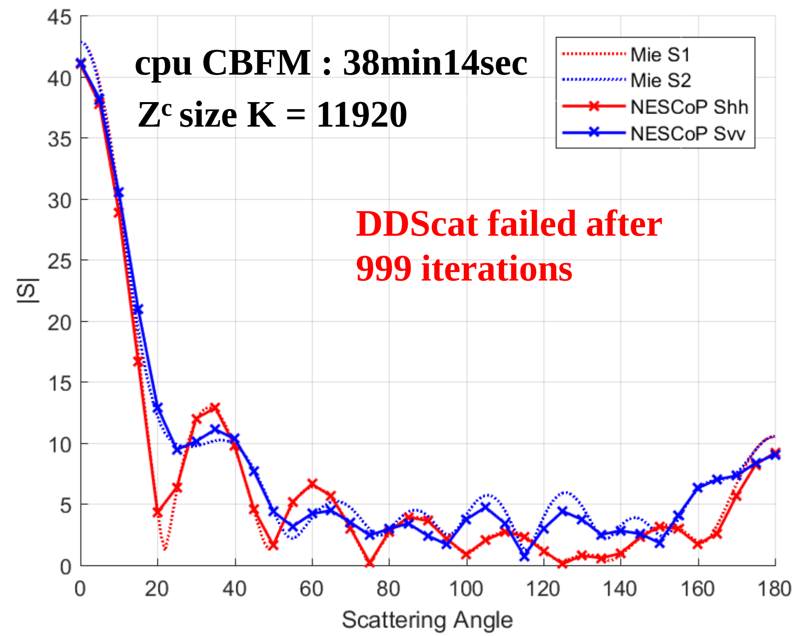


```
>QMRCCG IT=       998 f.err= 2.436E-01
>QMRCCG IT=       999 f.err= 2.436E-01

real  25m39.069s
```

Ice-phase particle modeling : OpenSSP database

OpenSSP database

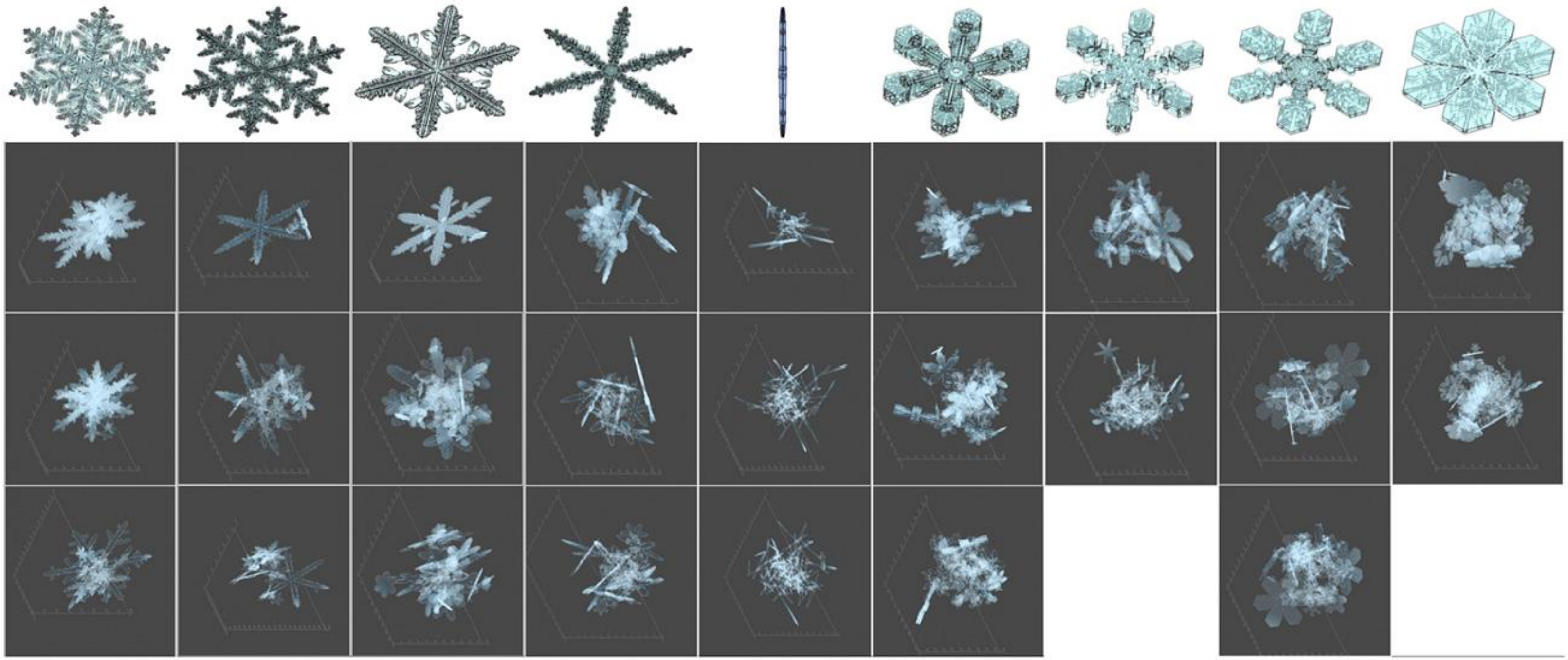

(top) Pristine crystal types simulated using the snowfake algorithm [adapted from Gravner and Griffeath (2009)]. Beneath each type are snapshots of the aggregation simulation that is based upon each crystal type.

[1] Kuo, K. S., Olson, W. S., Johnson, B. T., Grecu, M., Tian, L., Clune, T. L., ... & Meneghini, R. (2016). The Microwave Radiative Properties of Falling Snow Derived from Nonspherical Ice Particle Models. Part I: An Extensive Database of Simulated Pristine Crystals and Aggregate Particles, and Their Scattering Properties. Journal of Applied Meteorology and Climatology, 55(3), 691-708.

ftp://gpmweb2.pps.eosdis.nasa.gov/pub/OpenSSP/

- **6646 particles : single pristine crystals and aggregate snow particles**
- **50 µm resolution**

Numerical Analysis : NESCoP vs DDScat

a0072

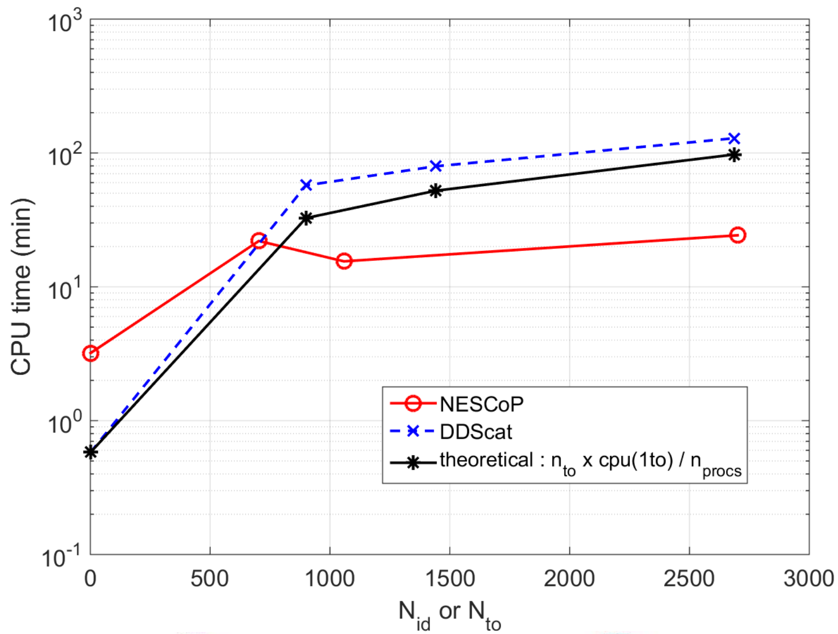

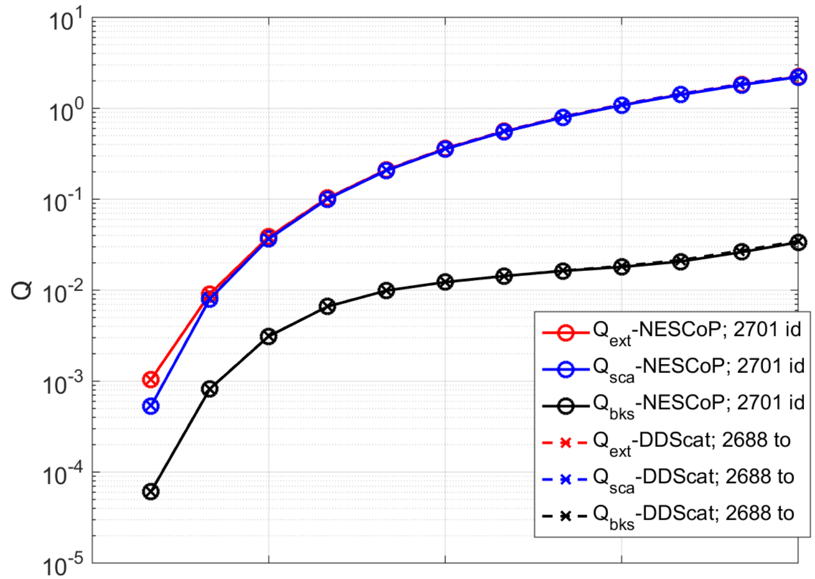

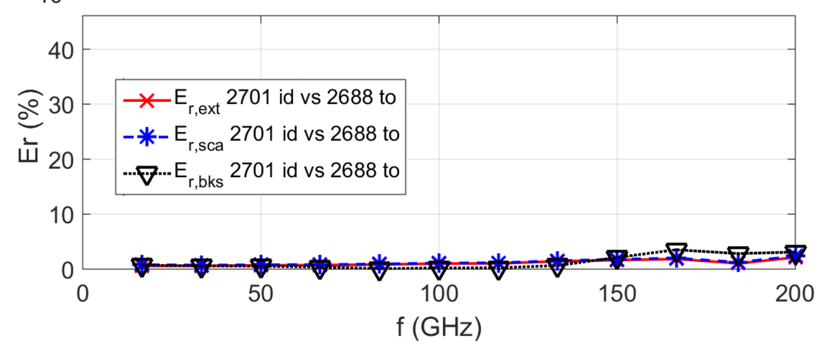

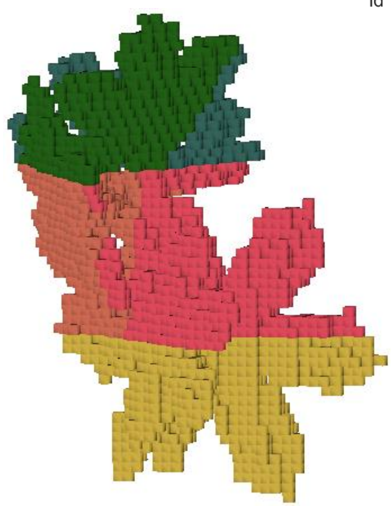

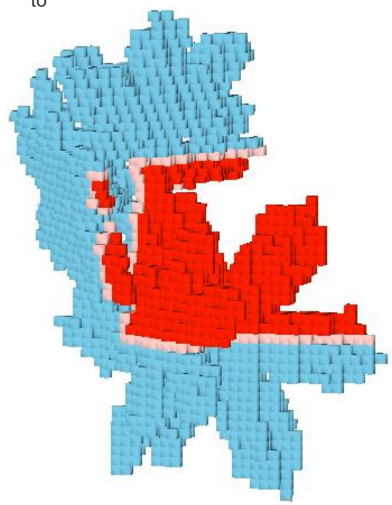

$a_{p,eff}$ = 0.5 mm; d_{max}=2.55 mm;
16 $\leq$f $\leq$ 200 Ghz $\rightarrow$ 0.17 $\leq$ x $\leq$ 2.09
and |m|kd $\leq$ 0.37; Nb_c=4159

Numerical Analysis : NESCoP vs DDScat

p08

N_{to}	N_β, N_θ, N_Φ	$E_{r,ext/scat}$	$E_{r,bks}$	time
2688	16, 12, 14	2.05	159.2	65.37
14520	22, 30, 22	2.32	127.9	274.9
14616	58, 36, 7	2.34	107.9	562.17
10000	10, 50, 20	2.37	63.19	199.78
12000	8, 60, 25	2.36	51.15	213.5
12000	30, 80, 5	2.39	18.6	607.32
5700	60, 95, 1	2.4	13.04	1182
7840	80, 98, 1	2.39	9.52	1974.6

Time (min) and maximum relative difference (%) obtained with DDScat for the ice pristine p08 in comparison to NESCoP with 2701 id, depending on the number of target orientations N_{to} and on their distribution.

$a_{p,eff}$ = 0.58 mm;
d_{max}=4.30 mm;
$0.2 \le x \le 2.49$
$|m|kd \le 0.37$;
Nb_c=6738

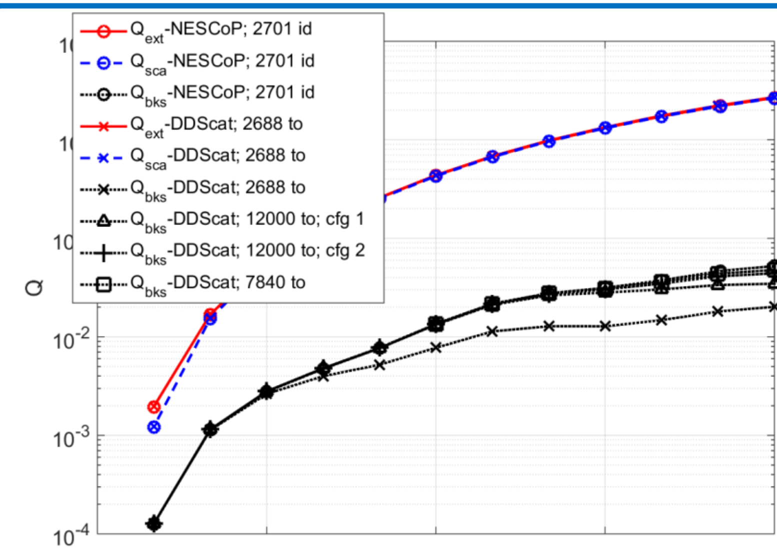

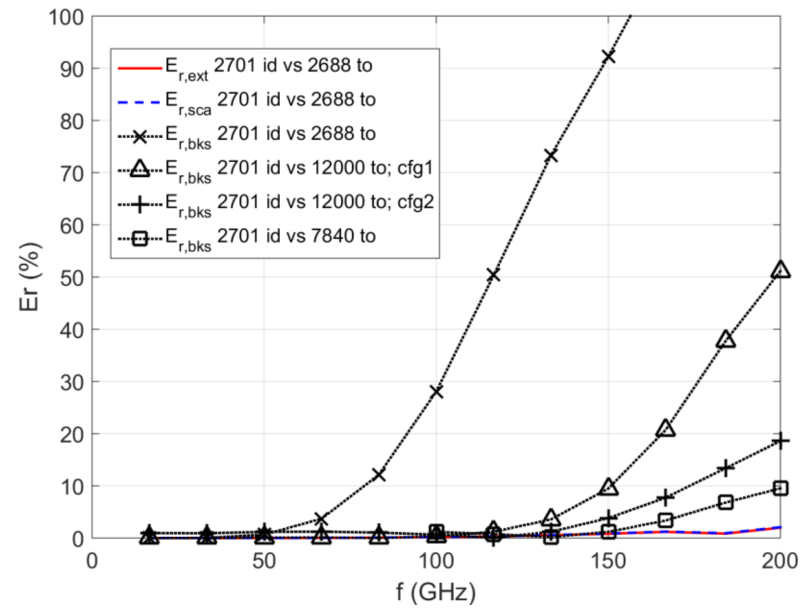

16

Numerical Analysis : NESCoP vs DDScat

a0058

1id/1to

f =200 GHz

d=50 µm

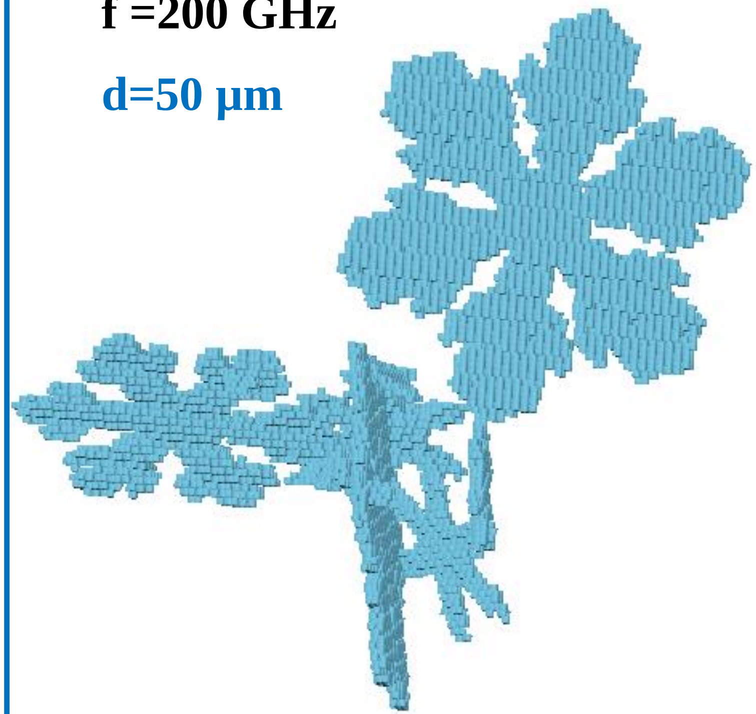

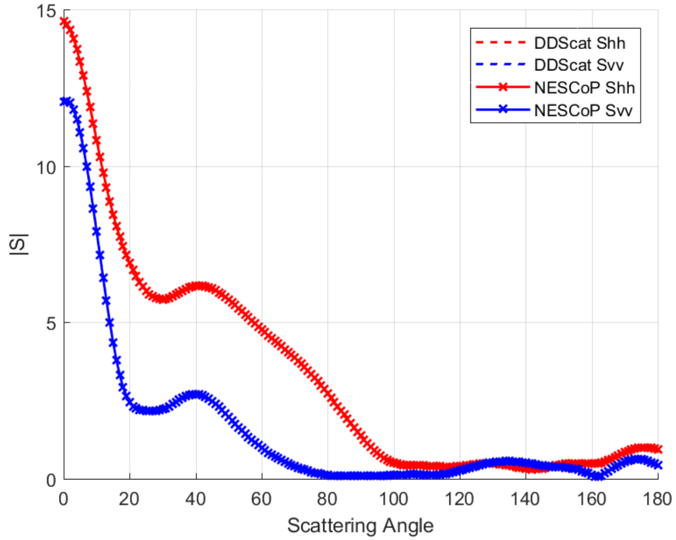

DDScat
1 min
18 sec

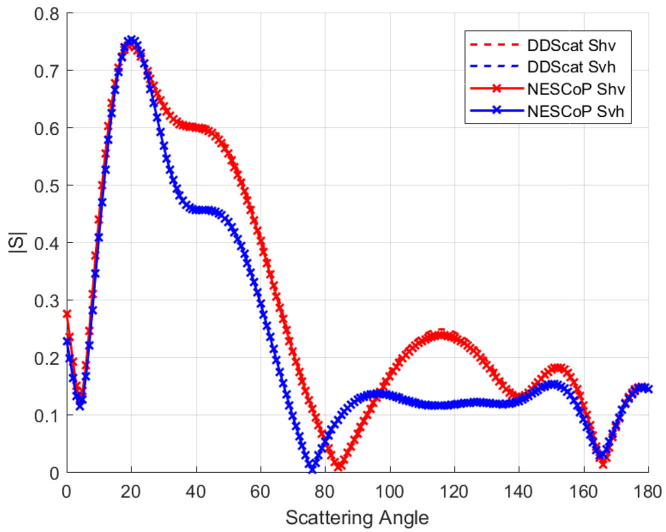

NESCoP
1 min
10 sec

d_{max}=5.6 mm;
x = 11.72;
$|m|kd = 0.37$; $D_\lambda = 16$
Nb_c =11148 cells

Numerical Analysis : NESCoP vs DDScat

a0058

f =659 GHz

d=17 μm

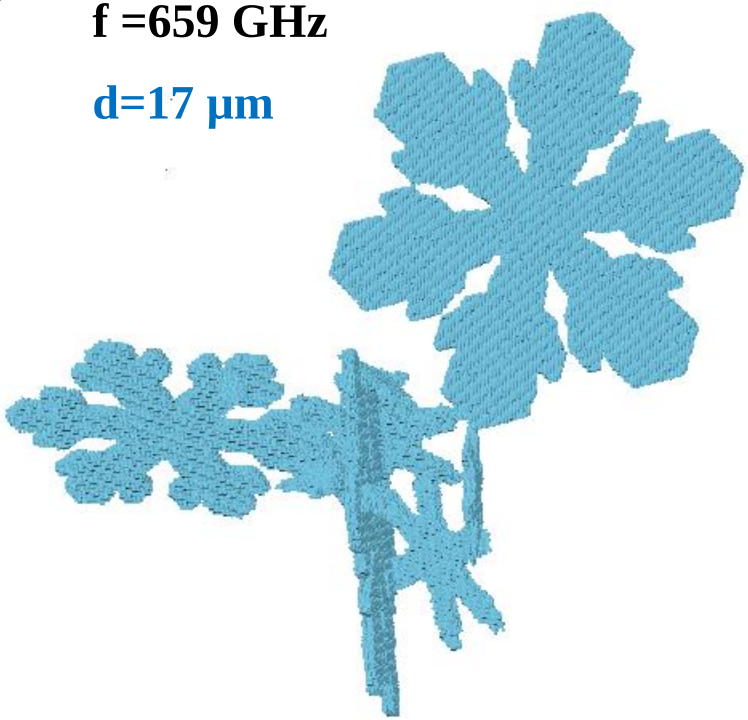

1id/1to

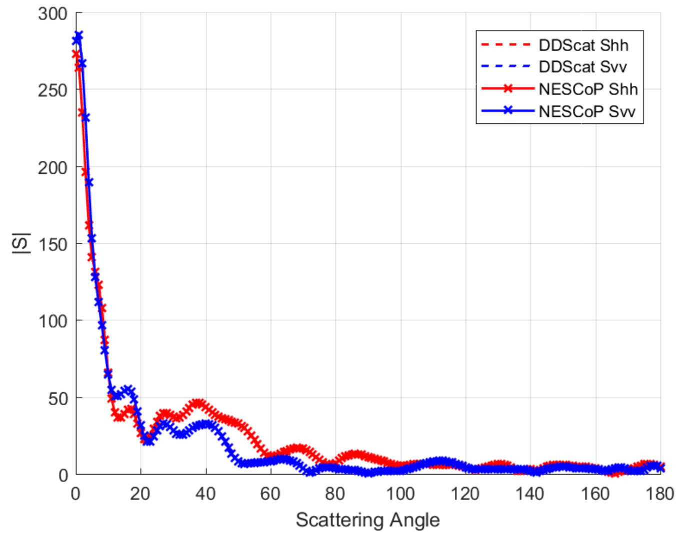

DDScat
16 h

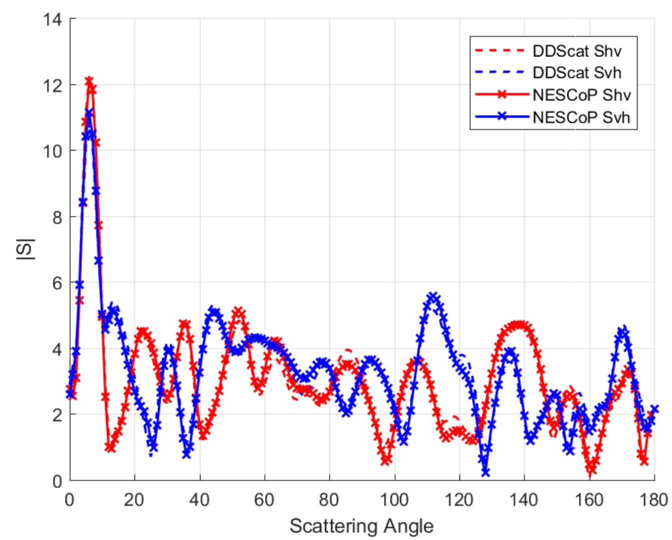

NESCoP
1 h 8 min

d_{max}=5.6 mm;
x = 38.66;
$|m|kd$ = 0.41; D_{λ} = 15
Nb_c =303034 cells

Numerical Analysis : NESCoP vs DDScat

a0058

Impact of d

f =200 GHz

d=50 µm
vs
d=17 µm

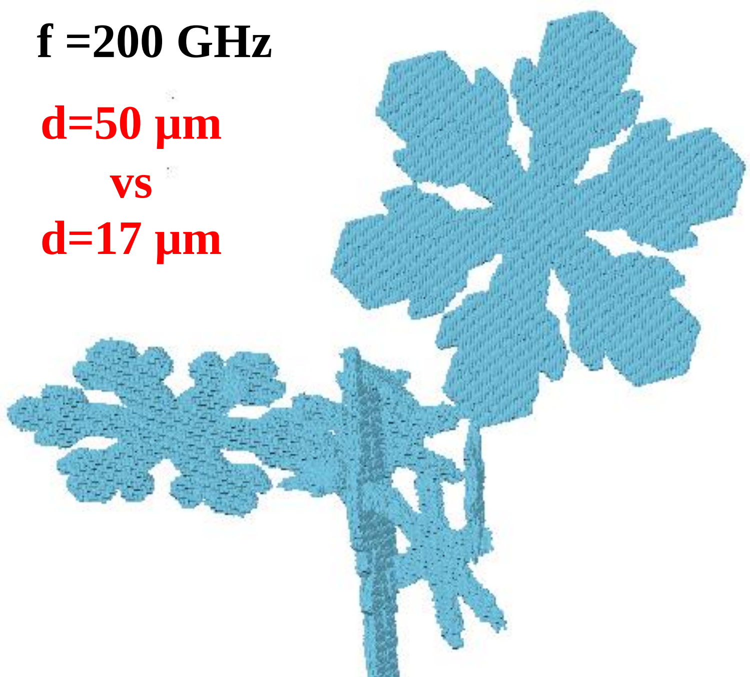

d_{max}=5.6 mm; x = 11.72;
|m|kd = 0.37; D_{λ} = 16
vs
|m|kd = 0.12; D_{λ} = 50

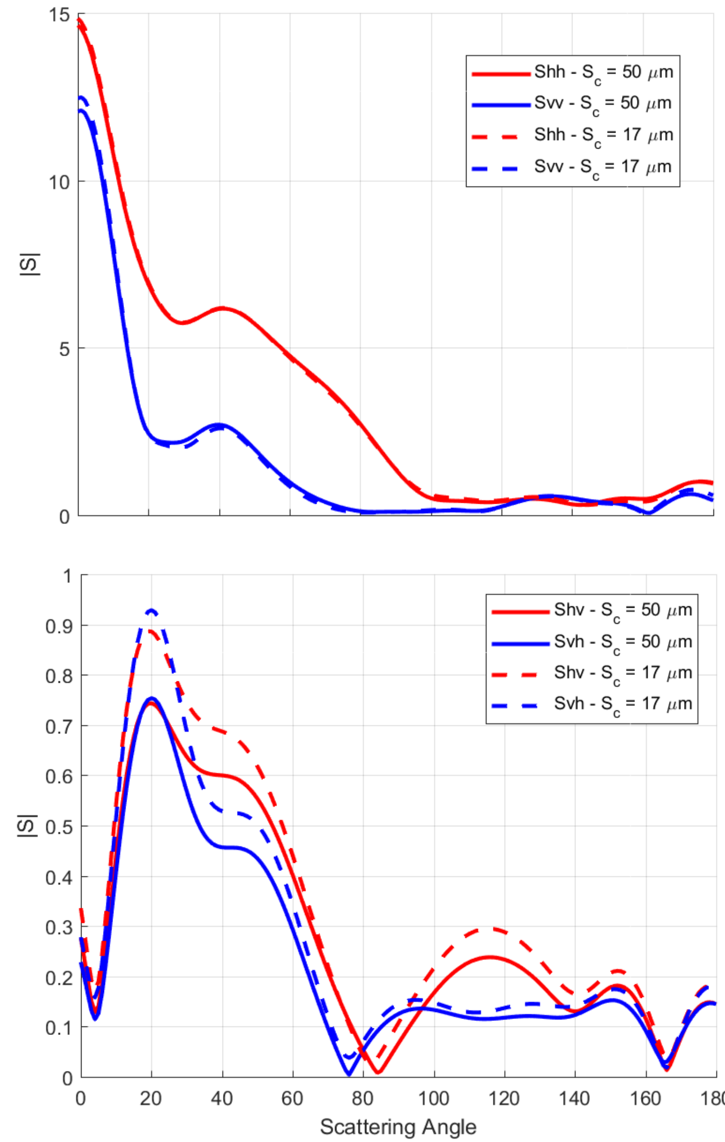

Numerical Analysis : NESCoP vs DDScat

a0006

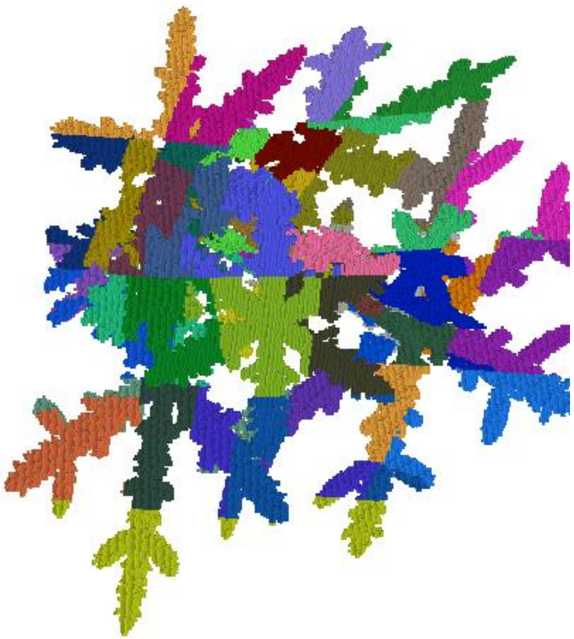

a_{eff} = 1.61 mm;
d_{max}=11.45 mm;
$2 \leq x \leq 24$
$|m|kd \leq 0.37$
Nb_c =140896 cells

180 to (N_θ=18; N_ϕ=10) / 1891 id (N_θ=31; N_ϕ=61)

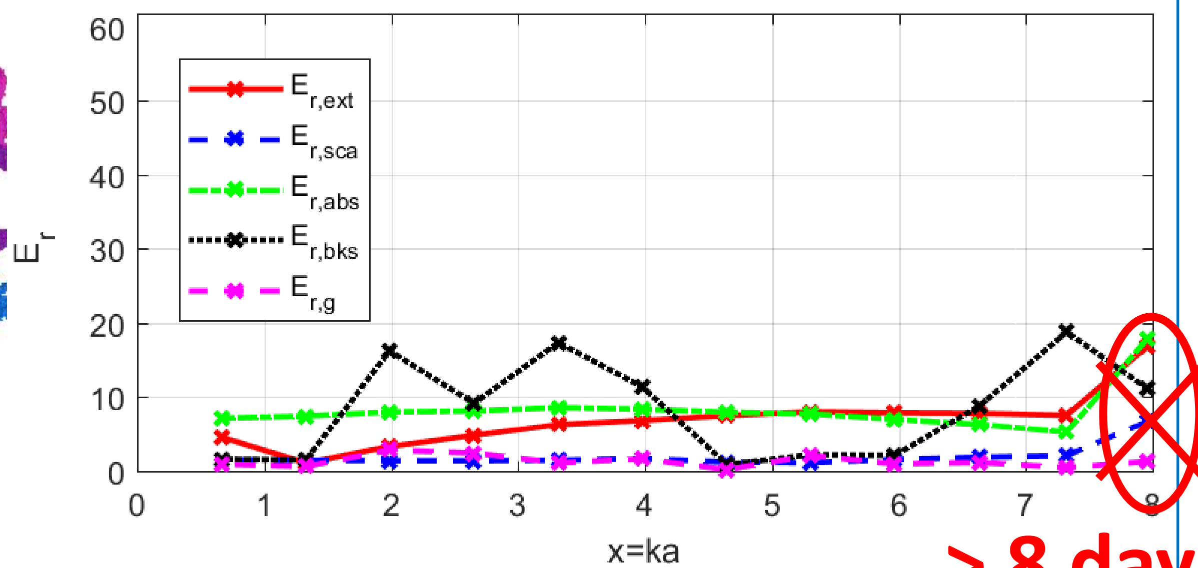

> 8 days

OpenMP; 64 GB of RAM; 16 cpus

DDScat (180 to)	190 id	703 id	1891 id
> 59 days	5 hours	12 hours	23 hours

Numerical Analysis : NESCoP vs DDScat

a0006

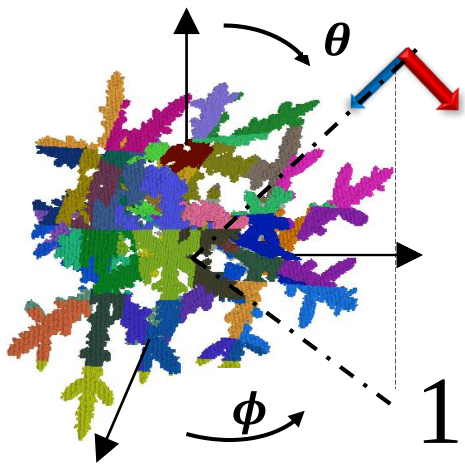

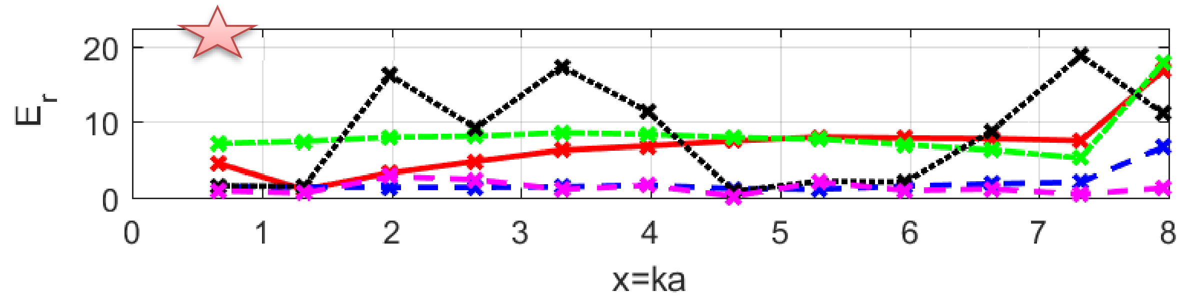

190 id

1891 id

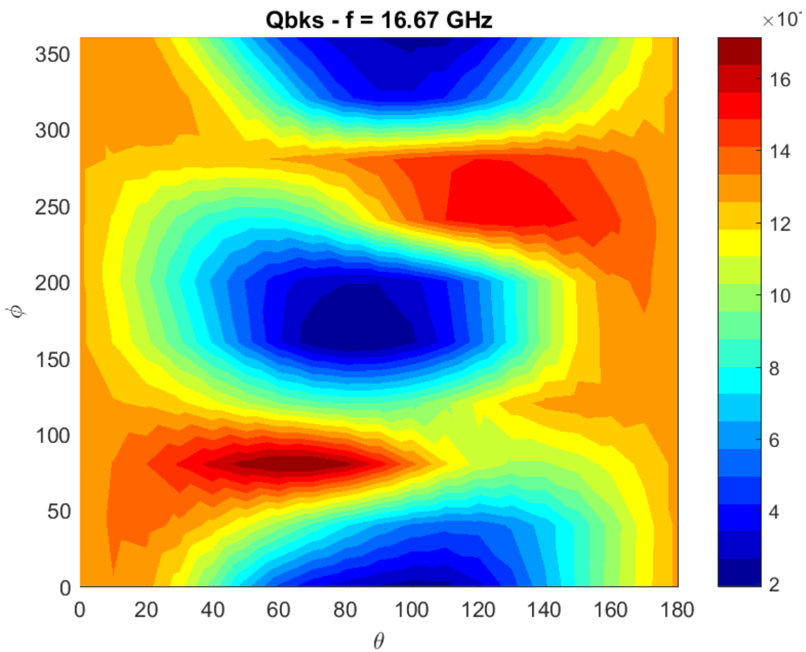

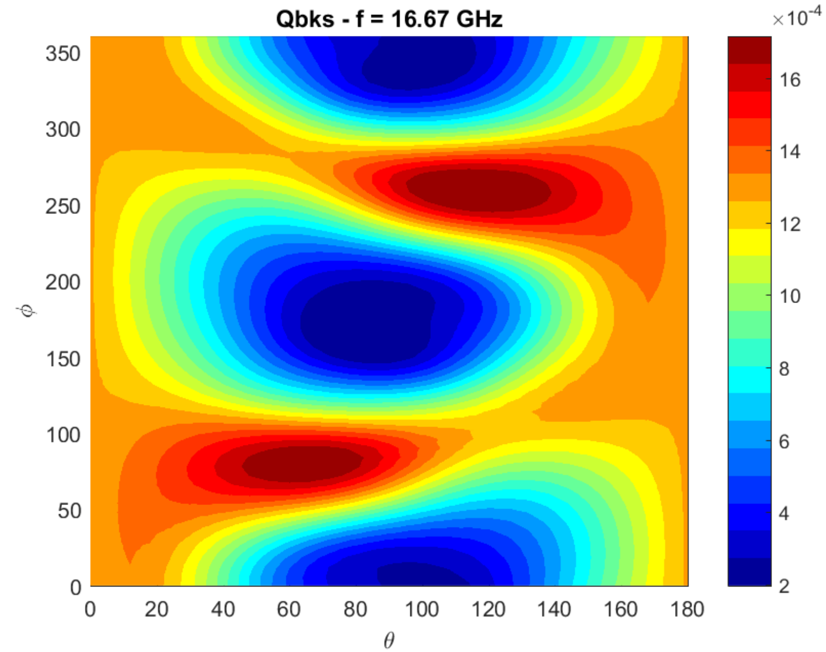

Numerical Analysis : NESCoP vs DDScat

a0006

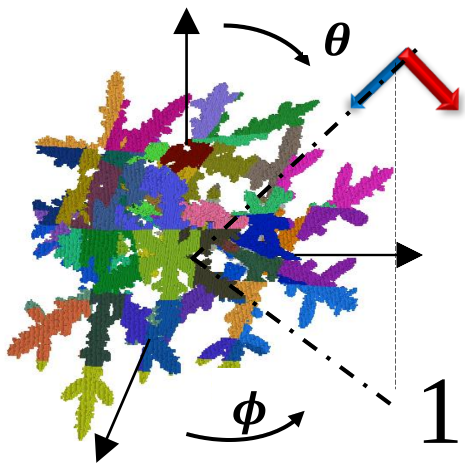

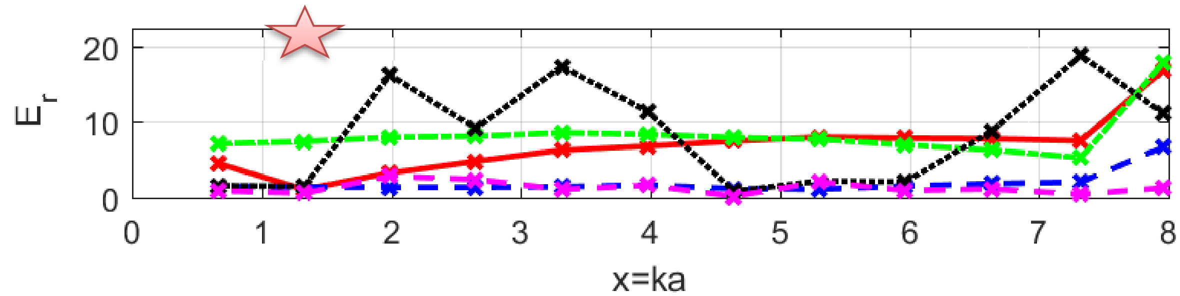

190 id

1891 id

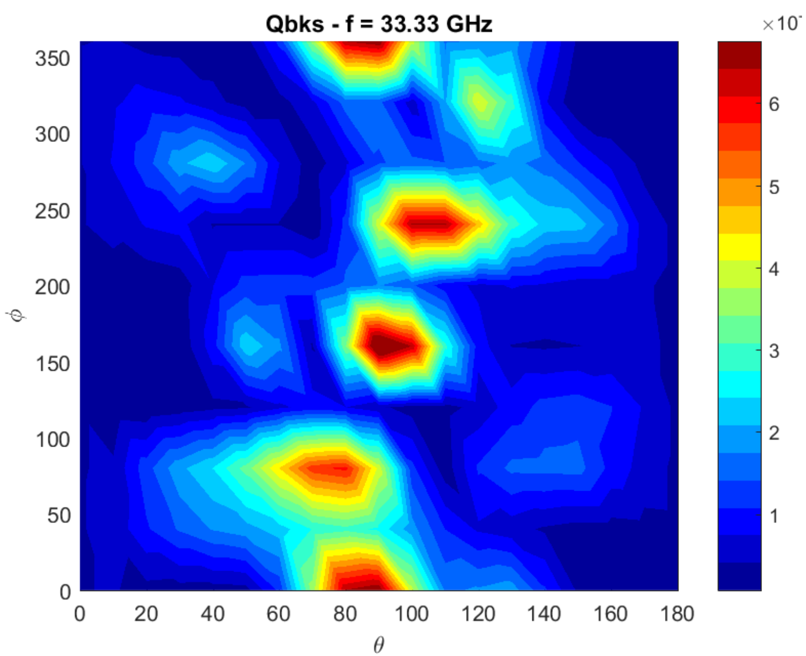

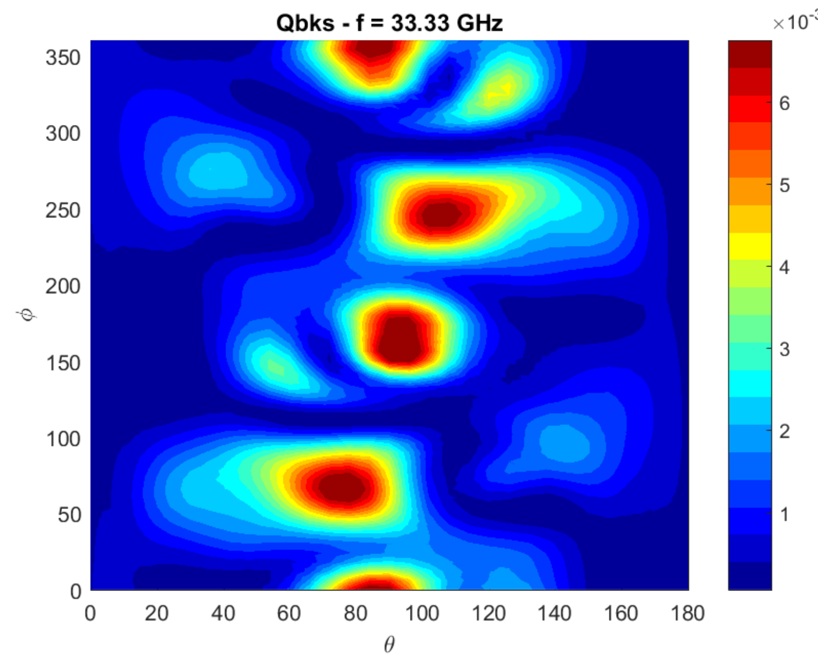

Numerical Analysis : NESCoP vs DDScat

a0006

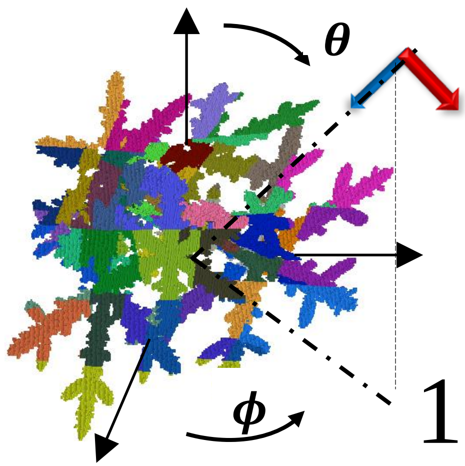

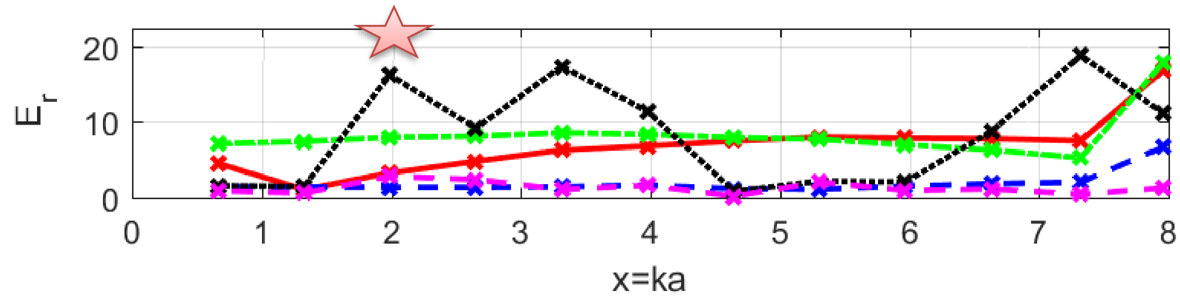

190 id

1891 id

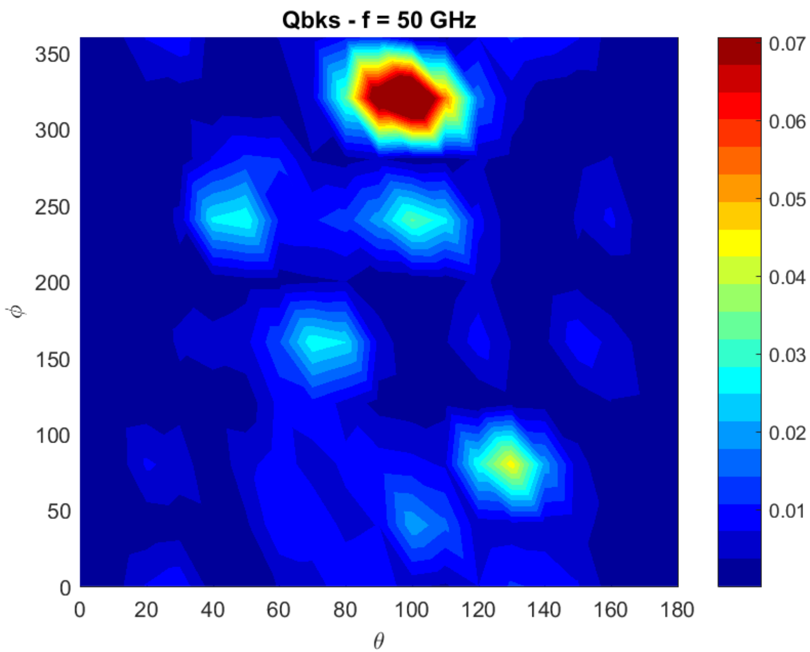

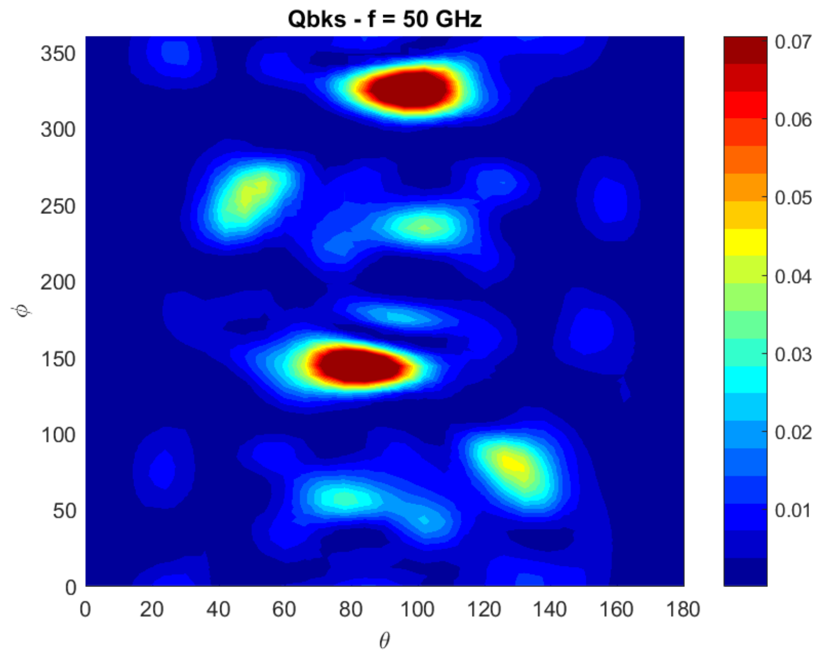

Numerical Analysis : NESCoP vs DDScat

a0006

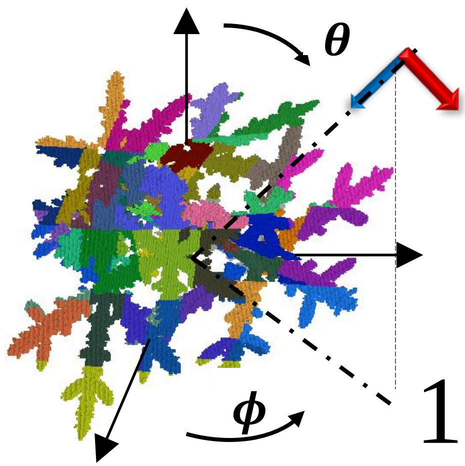

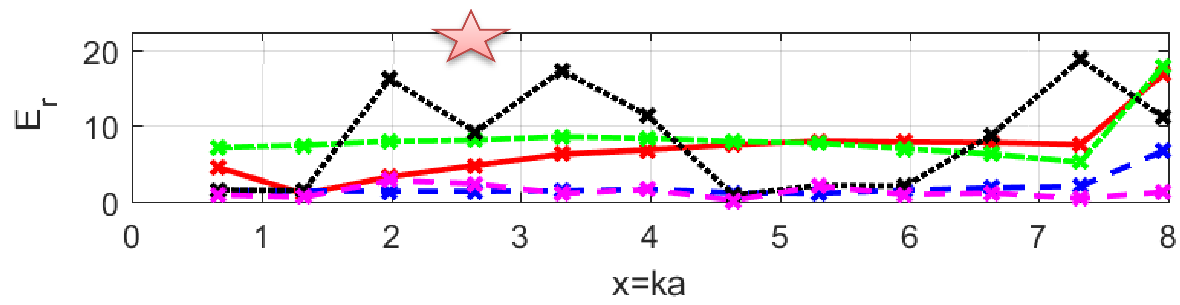

190 id

1891 id

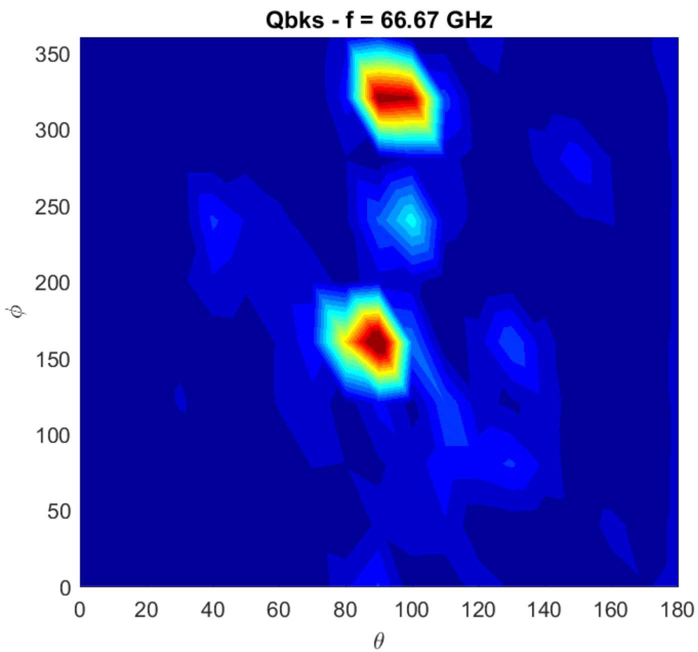

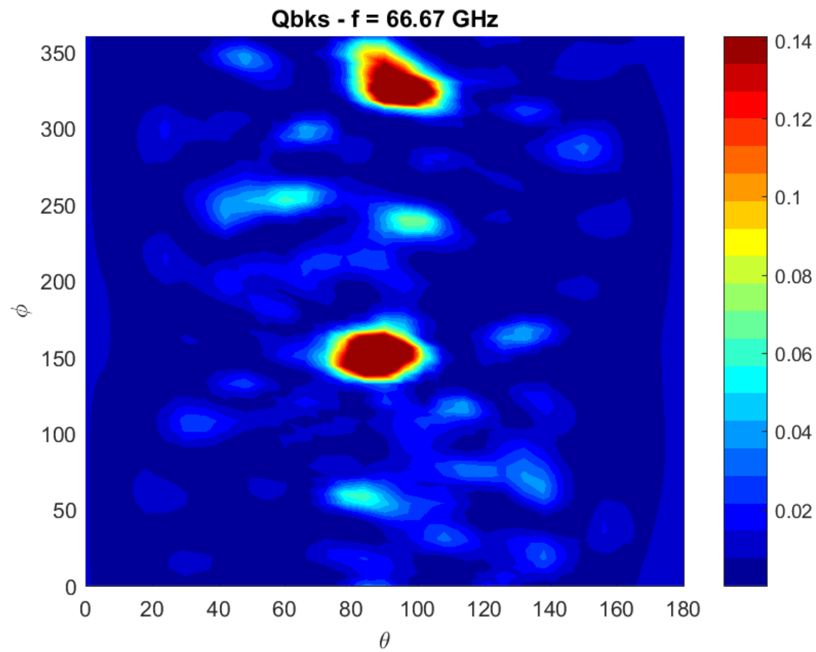

Numerical Analysis : NESCoP vs DDScat

a0006

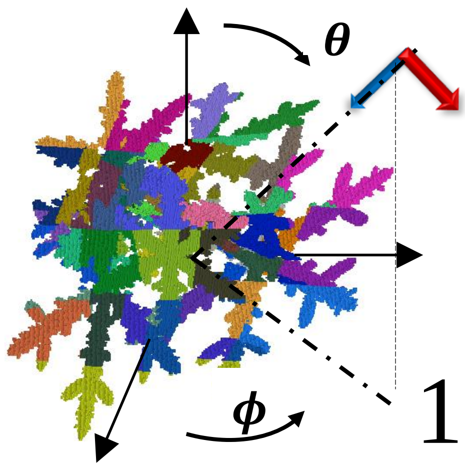

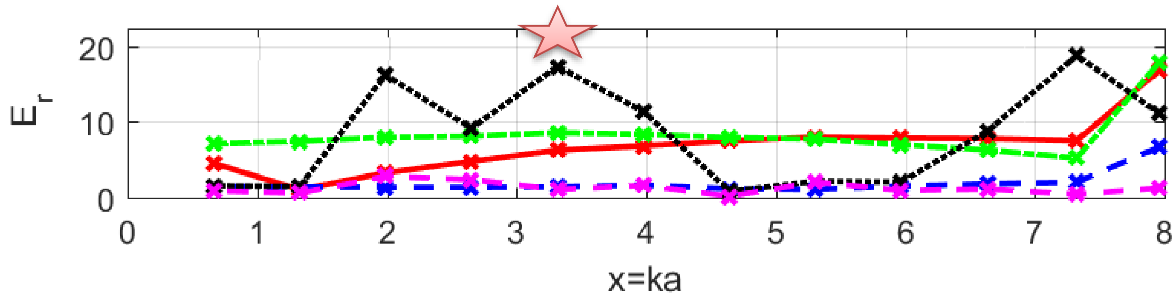

190 id

1891 id

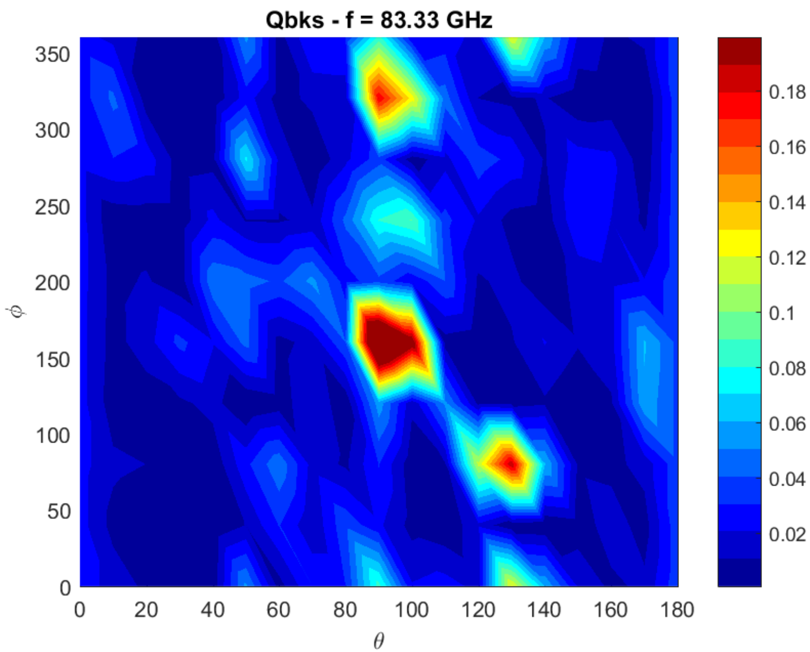

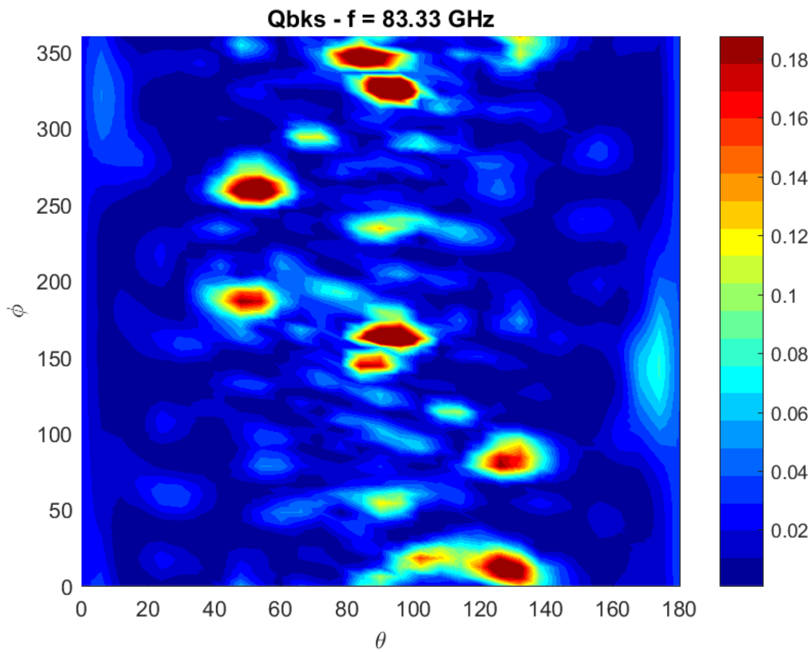

Numerical Analysis : NESCoP vs DDScat

a0006

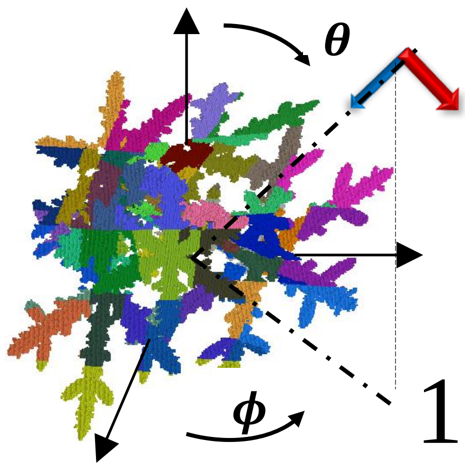

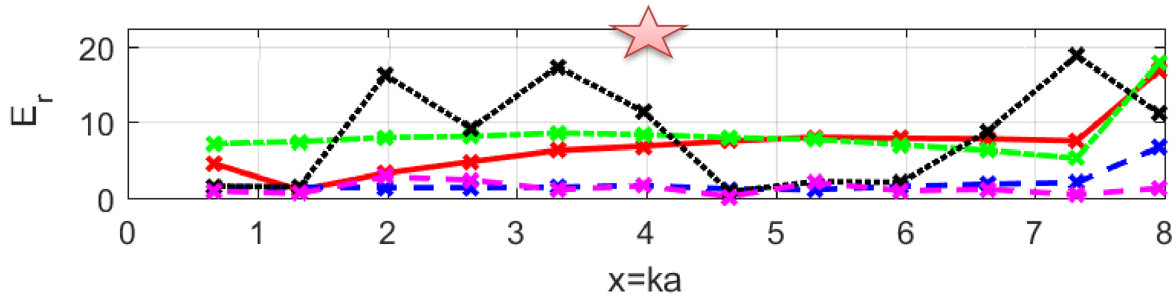

190 id

1891 id

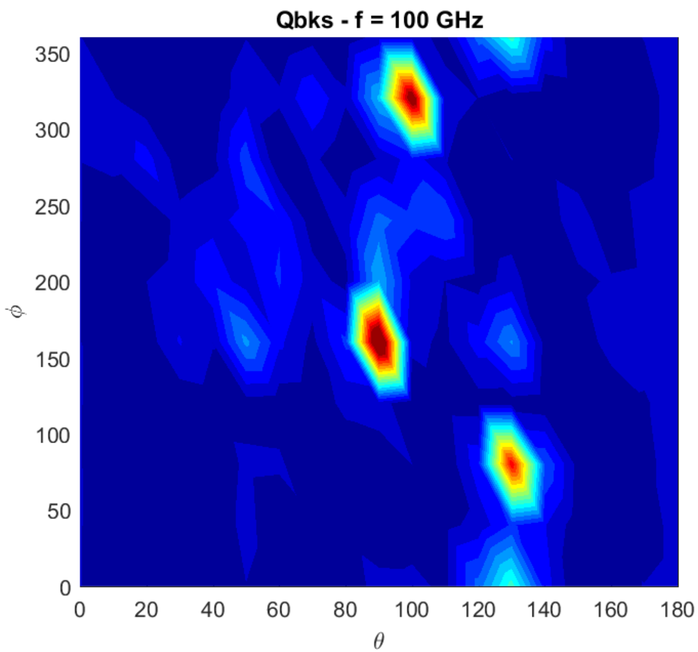

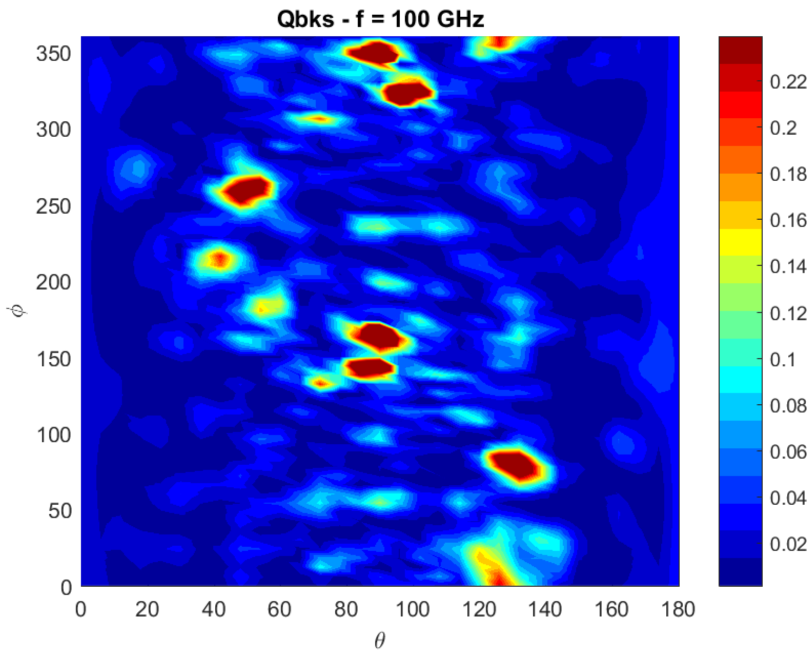

Numerical Analysis : NESCoP vs DDScat

a0006

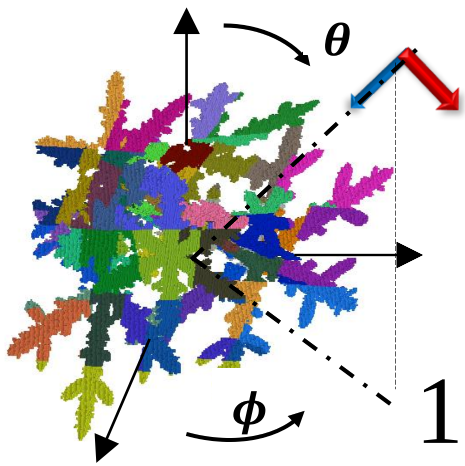

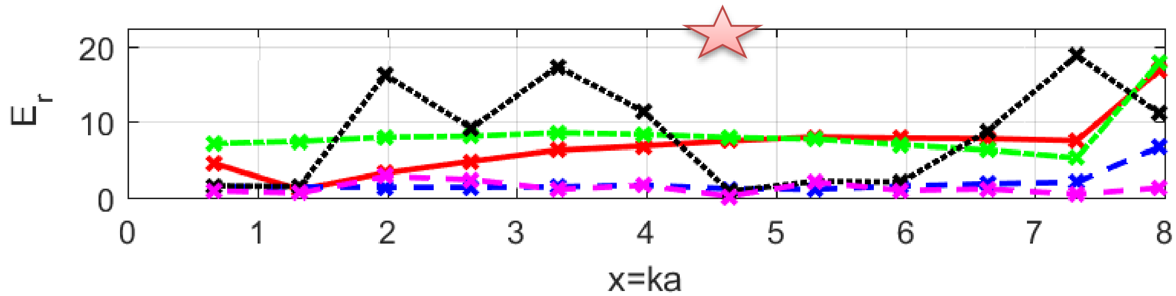

190 id

1891 id

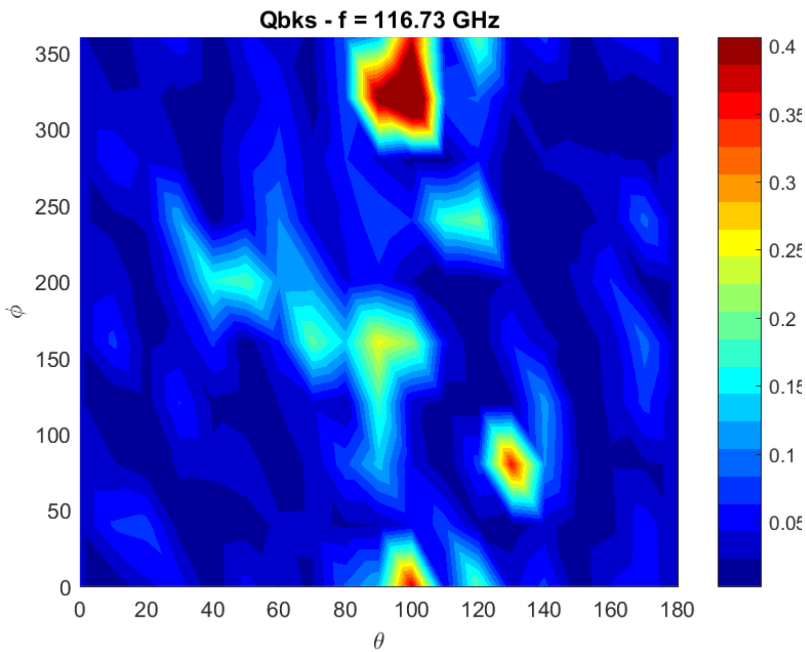

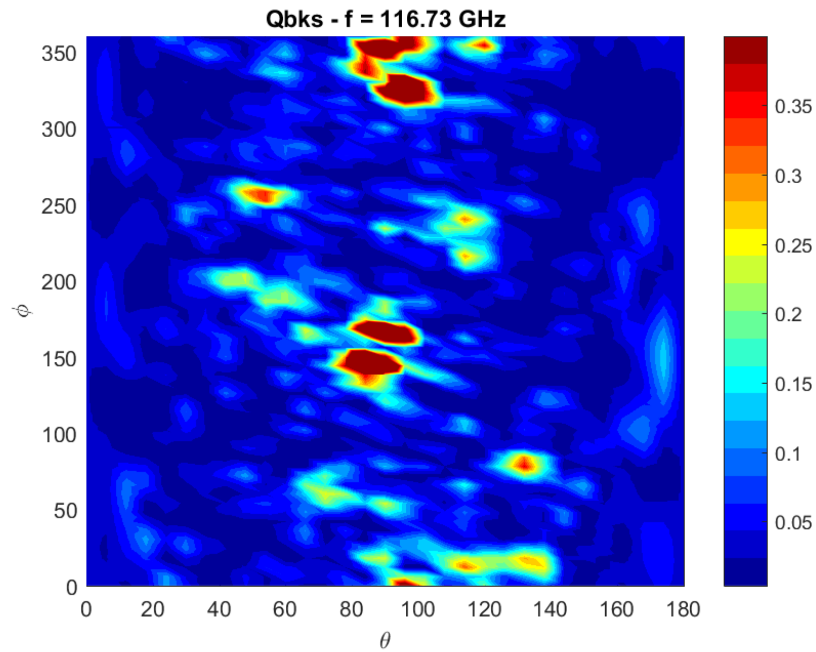

Numerical Analysis : NESCoP vs DDScat

a0006

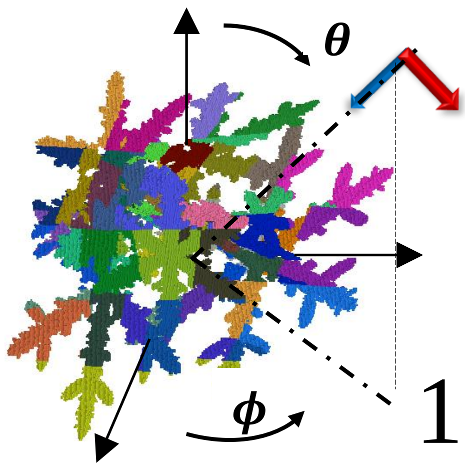

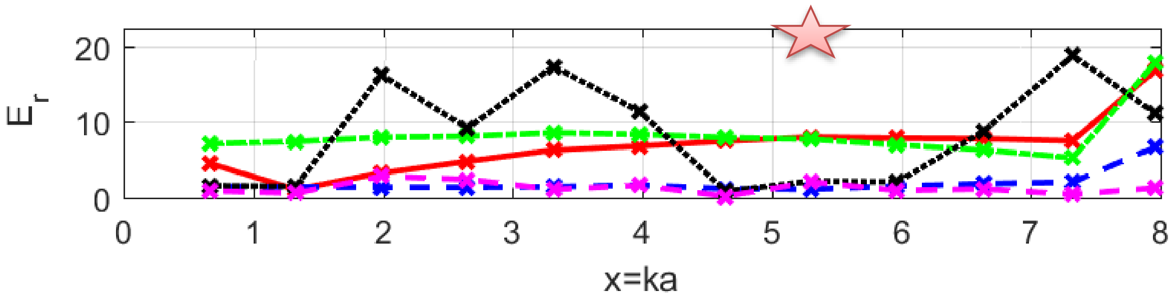

190 id

1891 id

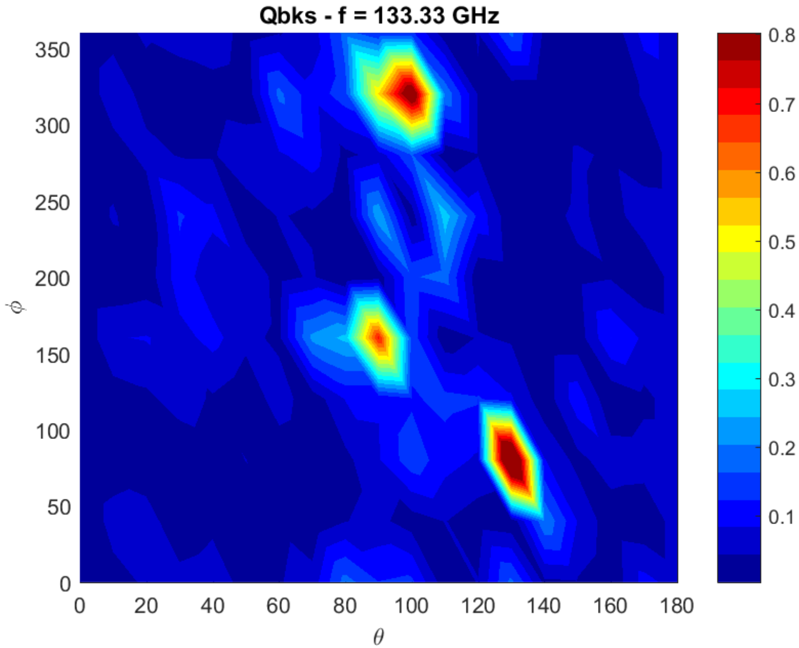

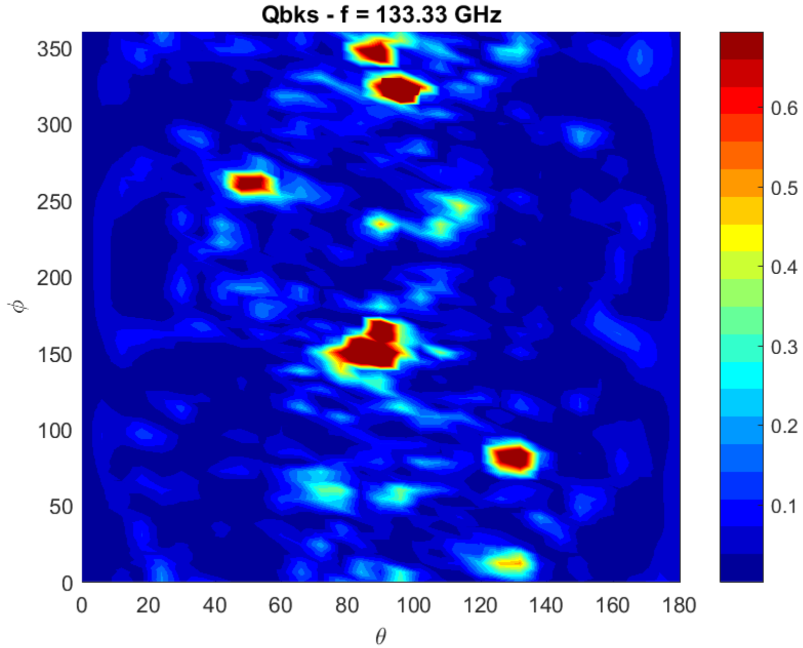

Numerical Analysis : NESCoP vs DDScat

a0006

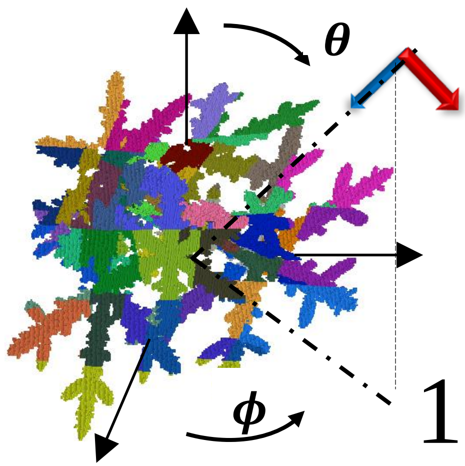

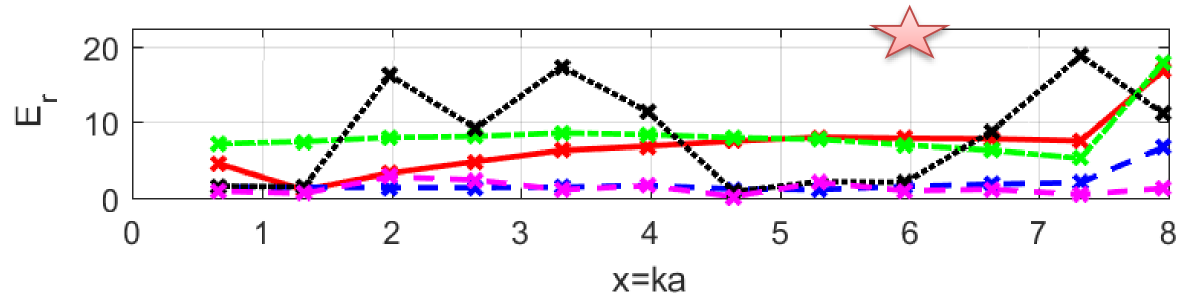

190 id

1891 id

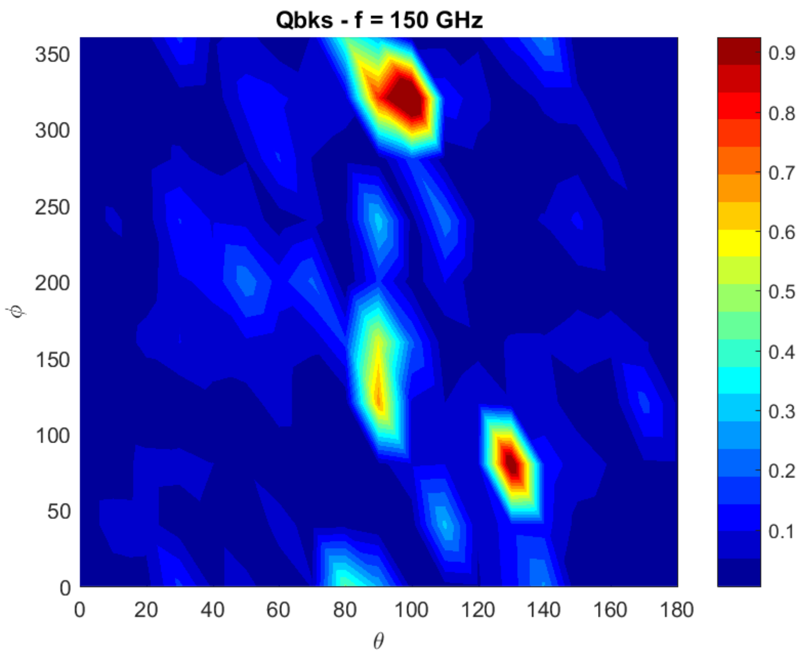

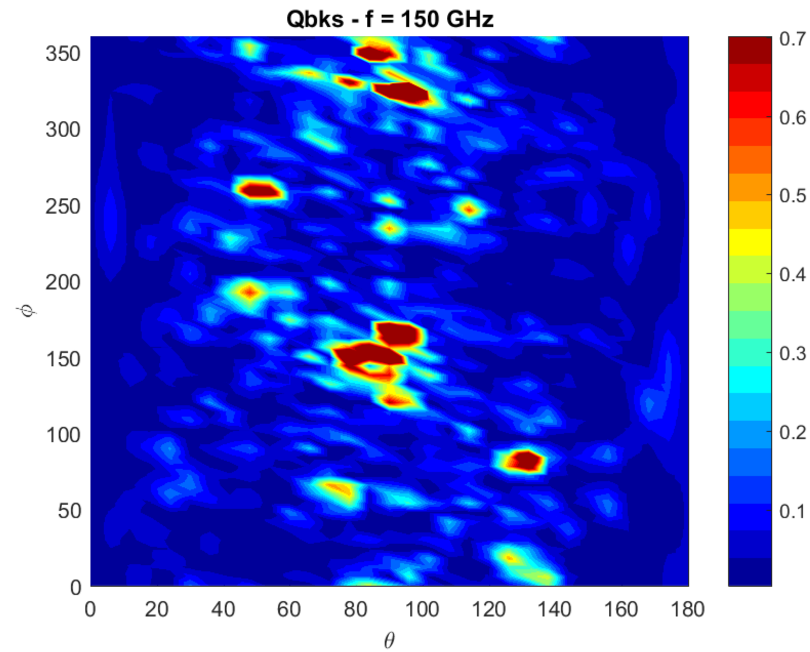

Numerical Analysis : NESCoP vs DDScat

a0006

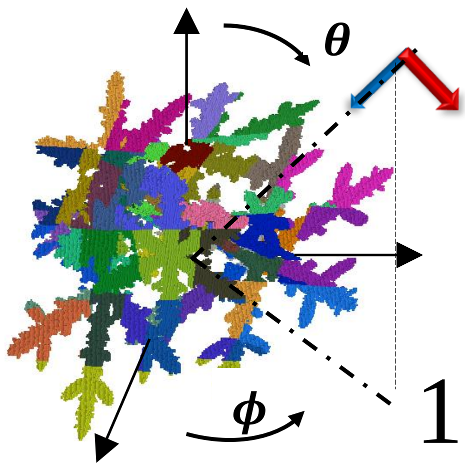

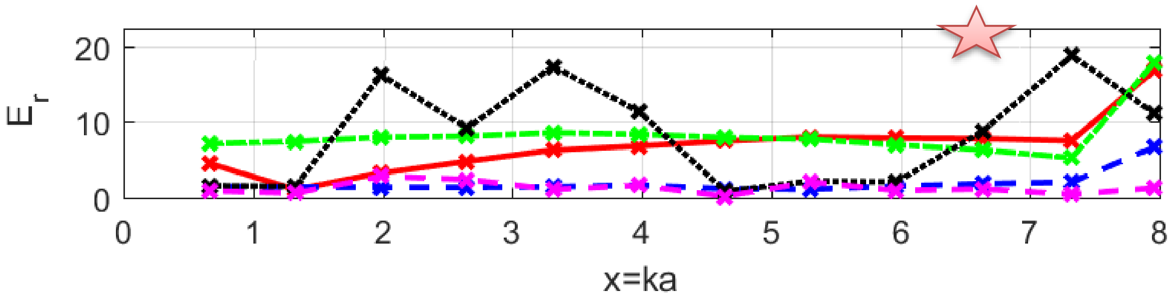

190 id

1891 id

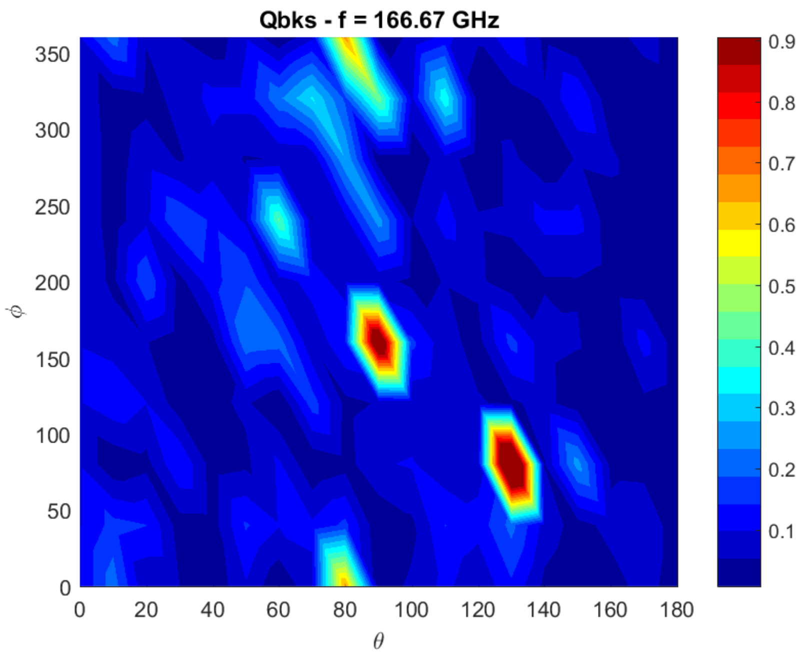

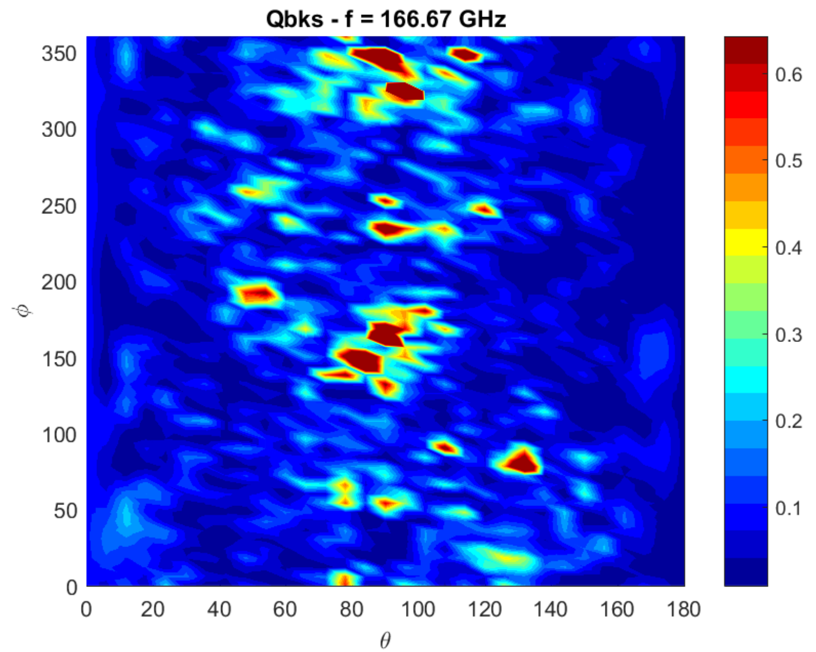

Numerical Analysis : NESCoP vs DDScat

a0006

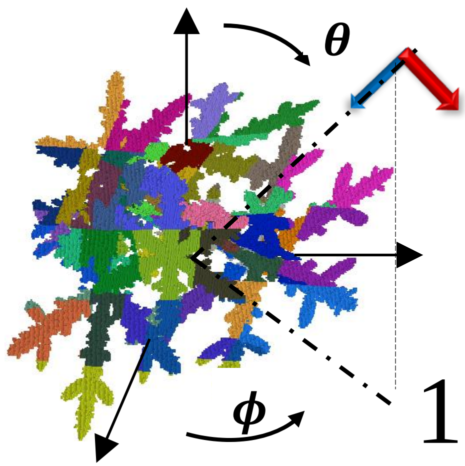

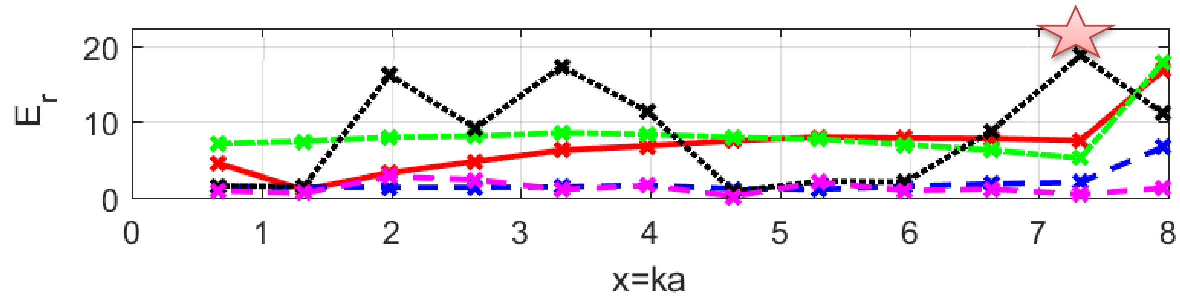

190 id

1891 id

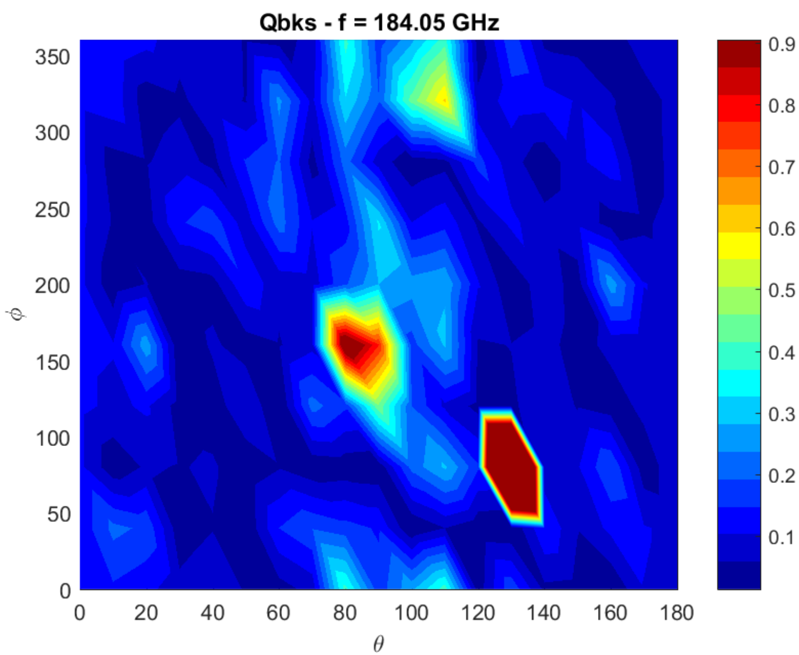

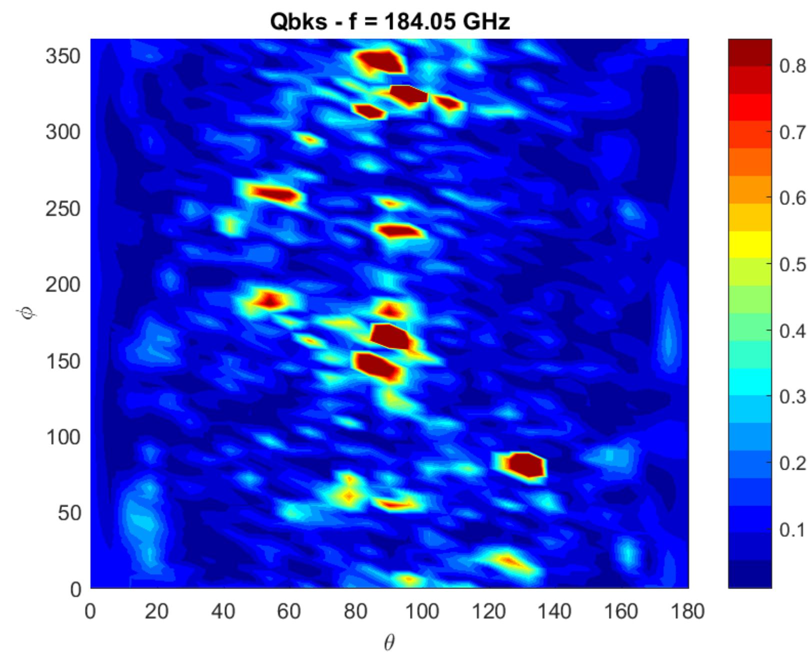

Numerical Analysis : NESCoP vs DDScat

a0006

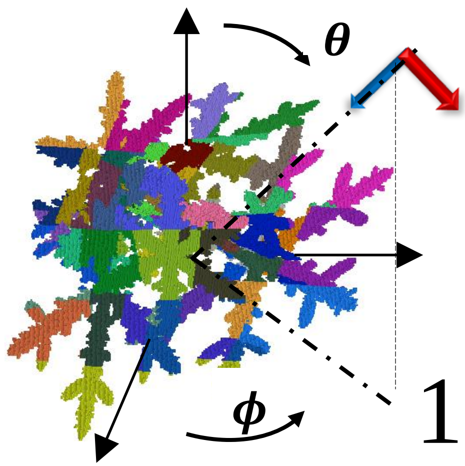

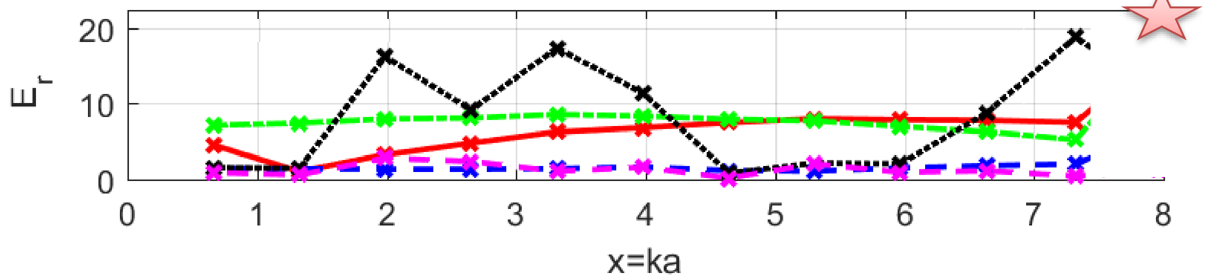

190 id

1891 id

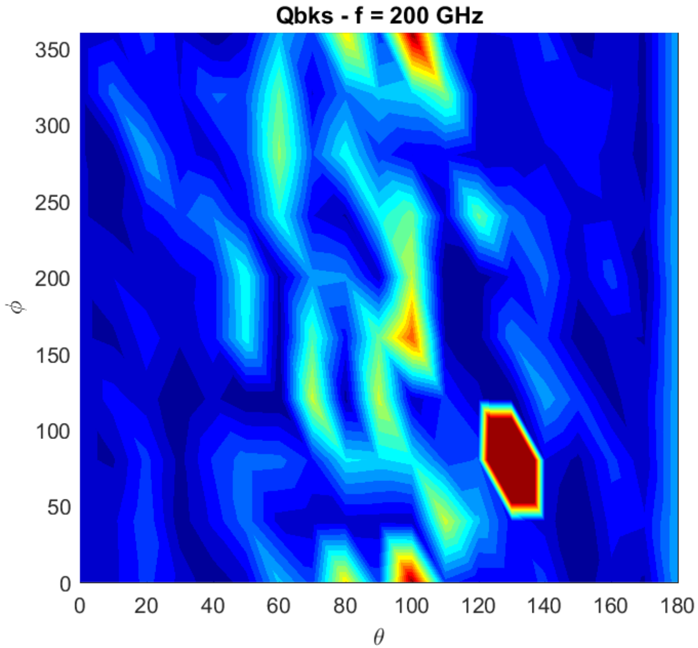

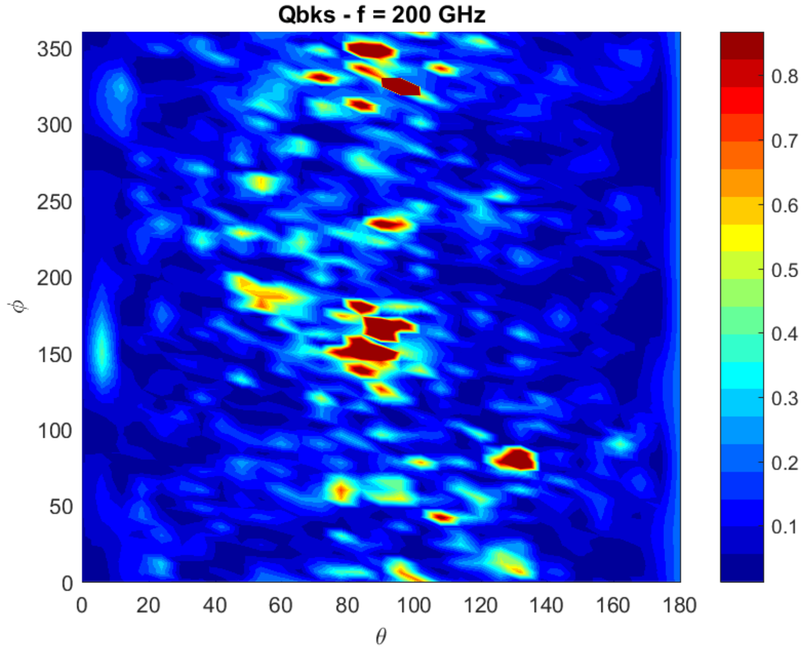

Conclusions and Perspectives

NESCoP

3D full wave model comparable to the DDA in terms of accuracy when providing **higher computational performance** particularly with orientational averaging of the EM scattering.

- ❖ MPI parallelization of the codes
- ❖ Exploring different techniques for efficient calculation of the CBFs
- ❖ Adaptation of the domain decomposition and CBFs calculation to 3D Chebyshev/Gaussian Random particles

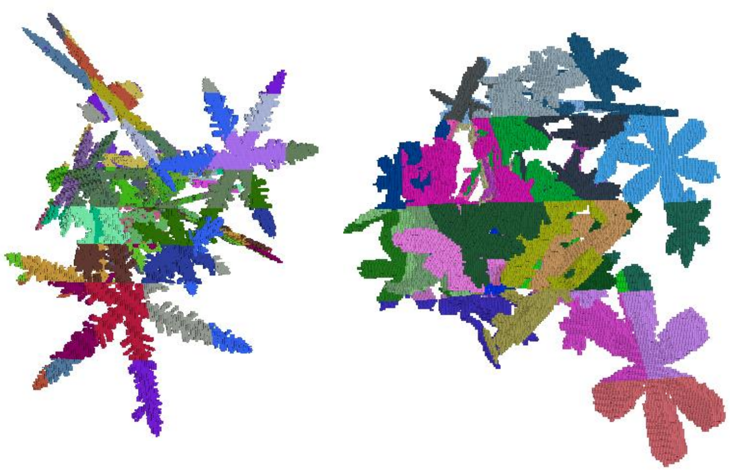

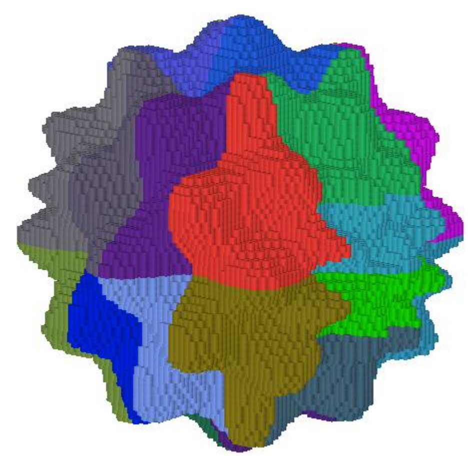

Thanks for your attention

Questions ?

Numerical Analysis : NESCoP vs DDScat

a0006

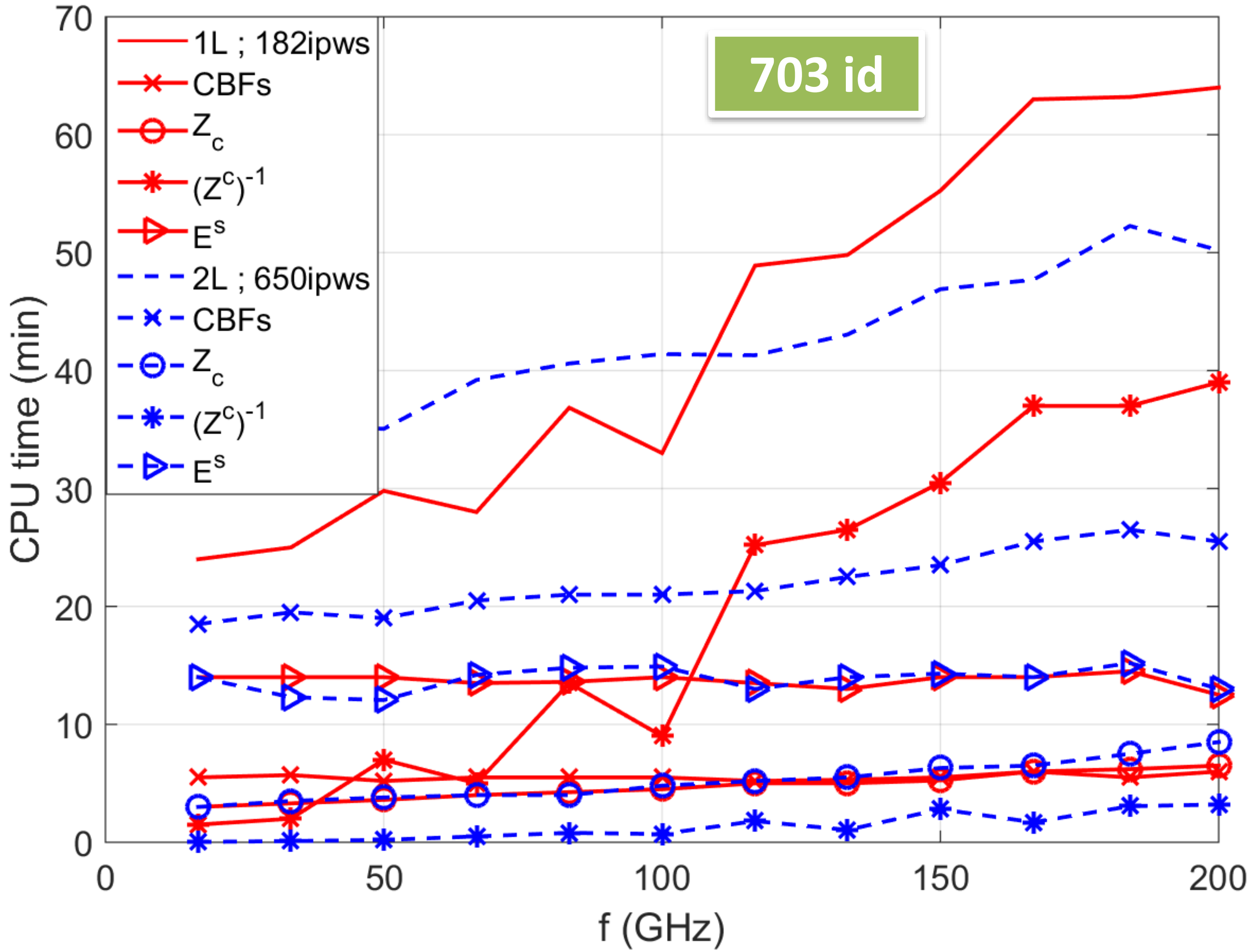

Numerical Analysis : NESCoP vs DDScat

a0006